AGU PUBLICATIONS

Journal of Advances in Modeling Earth Systems

RESEARCH ARTICLE
10.1002/2014MS000352

A multidecadal simulation of Atlantic tropical cyclones using a variable-resolution global atmospheric general circulation model

Colin M. Zarzycki[1] and Christiane Jablonowski[1]

[1]Department of Atmospheric, Oceanic, and Space Sciences, University of Michigan, Ann Arbor, Michigan, USA

Key Points:
- Variable-resolution models can improve the representation of tropical cyclones
- CAM produces realistic Atlantic TC climatology at 0.25° resolution
- Addition of local refinement in CAM does not impact synoptic scales

Correspondence to:
C. M. Zarzycki,
zarzycki@umich.edu

Citation:
Zarzycki, C. M., and C. Jablonowski (2014), A multidecadal simulation of Atlantic tropical cyclones using a variable-resolution global atmospheric general circulation model, *J. Adv. Model. Earth Syst.*, *6*, 805–828, doi:10.1002/2014MS000352.

Received 12 JUN 2014
Accepted 19 JUL 2014
Accepted article online 30 JUL 2014
Published online 12 AUG 2014

Abstract Using a variable-resolution option within the National Center for Atmospheric Research/Department of Energy Community Atmosphere Model (CAM) Spectral Element (SE) global model, a refined nest at 0.25° (∼28 km) horizontal resolution located over the North Atlantic is embedded within a global 1° (∼111 km) grid. The grid is designed such that fine grid cells are located where tropical cyclones (TCs) are observed to occur during the Atlantic TC season (June–November). Two simulations are compared, one with refinement and one control case with no refinement (globally uniform 1° grid). Both simulations are integrated for 23 years using Atmospheric Model Intercomparison Protocols. TCs are tracked using an objective detection algorithm. The variable-resolution simulation produces significantly more TCs than the unrefined simulation. Storms that do form in the refined nest are much more intense, with multiple storms strengthening to Saffir-Simpson category 3 intensity or higher. Both count and spatial distribution of TC genesis and tracks in the variable-resolution simulation are well matched to observations and represent significant improvements over the unrefined simulation. Some degree of interannual skill is noted, with the variable-resolution grid able to reproduce the observed connection between Atlantic TCs and the El Niño-Southern Oscillation (ENSO). It is shown that Genesis Potential Index (GPI) is well matched between the refined and unrefined simulations, implying that the introduction of variable-resolution does not affect the synoptic environment. Potential "upscale" effects are noted in the variable-resolution simulation, suggesting stronger TCs in refined nests may play a role in meridional transport of momentum, heat, and moisture.

1. Introduction

With tropical cyclones currently estimated to be responsible for 19,000 fatalities and $26 billion in damages per year worldwide [*Mendelsohn et al.*, 2012], future projections of tropical cyclone (TC) activity continue to be an important research question in the climate modeling community. Simulating TCs in global atmospheric general circulation models (GCMs) is extremely difficult because they operate on small spatial scales. Fine horizontal grid spacings and, subsequently, significant computational resources are required. Global models used for recent climate assessments exhibited tropical cyclone intensity statistics which were biased weak since models cannot adequately resolve the dynamics of these features [*Hamilton*, 2008; *Flato et al.*, 2013]. Improvements in the community's ability to model these storms is of vital importance to lowering projection uncertainty and providing a more thorough picture of tropical cyclones' connection to the climate system.

Recent advances in computational ability have allowed for global simulations at relatively high (sub-50 kilometer) horizontal resolution. This increased resolution has produced significantly more realistic storm counts when compared to models with coarser grid spacing [*Oouchi et al.*, 2006; *Bengtsson et al.*, 2007; *Zhao et al.*, 2009; *Murakami et al.*, 2012; *Manganello et al.*, 2012; *Satoh et al.*, 2012; *Strachan et al.*, 2013; Wehner et al. (The effect of horizontal resolution on simulation quality in the Community Atmospheric Model, CAM5.1, submitted to *Journal of Advances in Modeling Earth Systems*, 2014)]. However, even with improved counts at the global scale, simulation of Atlantic TCs has continued to be particularly difficult. Model climatology is typically less skillful than in other ocean basins, even in models utilizing higher resolution [*Walsh et al.*, 2013].

The development of variable-resolution grids in conjunction with next generation models can allow for the selective application of high resolution in specific geographic regions, thereby improving both short-term predictions and long-term projections of tropical cyclones on parallel computing architectures. Variable-resolution general circulation models (VRGCMs) are similar to regional climate or limited area models

(LAMs). They nest a high-resolution domain over a specific area of interest, saving computational time which would have otherwise been used to simulate the remainder of the globe at high resolution. However, LAMs require lateral boundary conditions, which may come from a very different model, may suffer from interpolation error, and may be mathematically inconsistent, among other issues [*Warner et al*., 1997; *Mesinger and Veljovic*, 2013]. VRGCMs avoid these inconsistencies.

VRGCMs possess the ability to simulate the atmosphere at multiple resolutions and can serve as the intermediary tool between fixed-resolution GCMs and LAMs. Such variable-resolution models span multiple scales in a single simulation, focus their computational (high resolution) efforts on a specific region while establishing two-way interactions in a numerically and physically consistent way. Decreased computational demand associated with variable-resolution models (when compared to a globally uniform simulation at resolution equal to that of the high-resolution nest) allows for longer integration times, finer grid spacing, or additional ensemble members for a fixed amount of computing capability.

While grid stretching techniques exist [e.g., *Côté et al*., 1993; *Abiodun et al*., 2008; *Tomita*, 2008; among others], the majority of VRGCMs make use of locally refined grids to embed the high-resolution domain. The past few years has seen a proliferation of new models capable of spanning multiple resolutions in a single simulation [e.g., *Ringler et al*., 2008; *Walko and Avissar*, 2011; *Skamarock et al*., 2012; *Harris and Lin*, 2013; *Zarzycki et al*., 2014a, 2014b] which utilize recent advancements in both computing power and subgrid parameterizations. Tropical cyclones are an excellent target for these variable-resolution frameworks given their resolution dependence and the fact that storms are localized to individual ocean basins. However, VRGCMs have only been used by *Chauvin et al*. [2006] and *Caron et al*. [2011] for long-term studies of regional tropical cyclone climatology.

In this paper, we explore climate simulations using a variable-resolution implementation of the Community Atmosphere Model (CAM) with a Spectral Element (SE) dynamical core [*Neale et al*., 2010]. This model has been jointly developed by the National Center for Atmospheric Research (NCAR) and U.S. Department of Energy (DoE) laboratories. A high-resolution nest is embedded over the Atlantic Ocean. We discuss the implications of this refinement on tropical cyclone statistics in a multidecadal climate simulation using prescribed sea surface temperatures (SSTs) and sea ice. This experiment follows protocols outlined in the Atmospheric Model Intercomparison Project (AMIP) [*Gates*, 1992]. We seek to determine whether refinement provides a substantial increase in model skill in simulating tropical cyclones at the regional level, while not requiring the computing resources of a globally uniform, high-resolution grid. We also compare the performance of a refined grid to an unrefined grid to determine if tropical cyclones generated outside the nest are impacted by the addition of the high-resolution patch.

Section 2 offers an introduction to CAM-SE and its variable-resolution option as well as details regarding the climate simulation. Section 3 outlines the method used to detect tropical cyclones in model data. Section 4 explores the results of the simulations by investigating spatial climatology, count statistics, intensity profiles, and model variability of cyclone activity at the seasonal and interannual time scales. The findings of the study are discussed in section 5 and future areas of research pertaining to tropical cyclones and VRGCMs are suggested.

2. Variable-Resolution in CAM-SE

The atmospheric model used for this study is the NCAR/DoE Community Earth System Model (CESM) version 1.1. CESM is a fully coupled, community model allowing for various configurations of multiple separate models (including atmosphere, ocean, land, and sea ice) to simulate global climate.

The atmospheric component within CESM is CAM. In particular, we utilize the CAM version 5 subgrid physical parameterization package [*Neale et al*., 2010] and the spectral element dynamical core [*Taylor et al*., 1997; *Taylor*, 2011; *Dennis et al*., 2012]. The SE dynamical core is the newest of the four dynamical cores available in CAM and replaced the Finite Volume (FV) option as the model default as of version 5.3, released in 2013. The spectral element scheme's mathematical compatibility allows for exact local conservation of mass, energy, and 2-D potential vorticity [*Taylor and Fournier*, 2010].

CAM-SE uses the spectral element method on a cubed-sphere grid to discretize in the horizontal direction [*Dennis et al*., 2012]. Cubed-sphere grids provide for quasi-uniform mesh spacing over the entire surface of

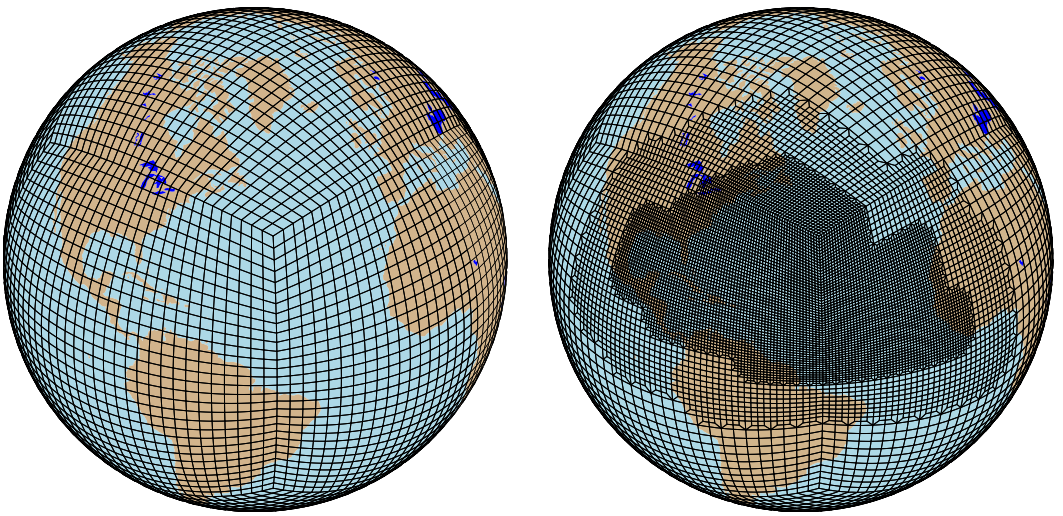

Figure 1. The two meshes used for this study are (a) a uniform 1° resolution mesh and (b) a variable-resolution mesh that ranges from 1° → 0.25°. Note that each element shown in the above plots contains additional 3 × 3 collocation cells.

the globe. This eliminates issues that arise from the use of traditional latitude-longitude grids such as the convergence of meridians in polar regions which requires either extremely short time steps or polar filtering to satisfy numerical stability constraints. The accuracy of the model can be controlled by selecting the polynomial degree of the basis functions on each quadrilateral element. The default polynomial degree in CAM-SE is selected to be three (cubic polynomials), leading to fourth-order spatial accuracy. We utilize a finite-difference approach in the vertical with a hybrid sigma-pressure coordinate, and a Runge-Kutta time discretization.

Spectral elements are highly localized numerical discretizations and therefore require minimal communication between processors on massively parallel computer systems. Therefore, it is an optimal choice for future, high-resolution climate simulations. *Dennis et al.* [2012] and *Evans et al.* [2013] have shown that CAM-SE outperforms other dynamical cores in CAM at all processor counts for 0.25° (∼28 km) resolution and finer and also scales nearly linearly up to one element per processor. As parallel computers continue to grow in size, CAM-SE is an attractive choice for high-resolution runs.

Because CAM-SE solves the hydrostatic primitive equations locally on individual elements, it possesses the ability to run on nonuniform grids without significant modifications to the underlying numerical scheme. The only two restrictions to running CAM-SE on nonuniform grids are that elements must be quadrilateral and the refinement must be conforming (meaning every edge is shared by exactly two elements). Any conforming tiling of the sphere with quadrilaterals that satisfies these two criteria is acceptable and allows CAM-SE to maintain key conservation properties on highly distorted grids.

To perform integrated climate simulations, CAM-SE is coupled to both an ocean/ice and land model through the CPL7 tri-grid coupler within the CESM framework [*Craig et al.*, 2012]. The coupler utilizes conservative remaps between model components to allow the atmosphere to run in conjunction with more standard ocean and land grids. Prescribed SSTs and sea ice concentrations are provided on a gx1v6 tripole grid (approximately 1°). The land model is the Community Land Model (CLM) version 4.0 run on a 0.9 by 1.25° latitude-longitude grid. Unlike the ocean/ice, the land model is not prescribed and is allowed to freely adjust.

We perform two identical simulations using two different atmospheric grids. The first is a globally uniform 1° (∼111 km) grid, seen in Figure 1a. This is also referred to as the "coarse" grid. The second is a grid with a global base resolution of 1° with a refined patch of 0.25° (∼28 km) grid cells centered over the North Atlantic Ocean (Figure 1b). This is referred to as the variable-resolution or "var-res" (VR) setup. Note that Figure 1 shows the elements which tile the sphere; each element contains an additional 3-by-3 grid of cells defined

Table 1. CAM-SE Resolutions of Interest to This Study[a]

Setup	Δx (°)	Δx (km)	Grid Elements (#)	Δt_{dyn} (s)	K_4 ($m^4\ s^{-1}$)
Uniform	1°	111	5400	360	1×10^{15}
Var-res	1° → 0.25°	111 → 28	13,340	100	$1 \times 10^{15} \rightarrow 1 \times 10^{13}$

[a]Grid spacing Δx (in kilometers and degrees) corresponds to the approximate grid spacing at the equator. Dynamics time steps (Δt_{dyn}) are globally constrained by the finest grid scale in an individual variable-resolution model simulation, while the fourth-order diffusion coefficient $K_4(\Delta x)$ (hyperdiffusion) is allowed to vary among individual elements.

by the spectral element method's collocation points which is used to define the effective horizontal resolution. In the variable-resolution model runs, there is a transition region of 0.5° between the global background grid and the main refinement area. The irregular shape of the high-resolution nest was selected to approximate the region where North Atlantic tropical cyclones occur in the historical record. A "2-refinement" structure is used to transition between resolutions, where a halving of grid spacing is achieved by dividing each cubed-sphere element into four equal elements with a one-element transition region in between [*Anderson et al*., 2009].

The variable-resolution grid in Figure 1b contains approximately one sixth of the number of grid cells as a globally uniform 0.25° mesh. Past work has shown that CAM-SE's performance scales linearly with the number of grid elements [*Dennis et al*., 2012; *Evans et al*., 2013; *Zarzycki et al*., 2014b] up to very large processor counts, so the variable-resolution mesh configuration is expected to reduce the runtime by a factor of 6 compared to a globally uniform high-resolution grid. Short, informal timing studies comparing a uniform 0.25° grid with the variable-resolution mesh show that this is a valid assumption, although components of CESM which are less scalable than CAM-SE result in a slight degradation of the linear speedup.

A comparison of the two model grids and their configuration is shown in Table 1. Explicit fourth-order hyperdiffusion is applied in each element and the diffusion coefficient is scaled according to grid spacing. A more detailed discussion about the hyperdiffusion can be found in *Zarzycki et al*. [2014a]. The number of vertical levels is 30. The physics time step is set to 1800 s instead of the 0.25° default of 450 s. *Williamson* [2013] showed that CAM's deep convective scheme becomes almost inactive at short physics time steps due to its inherent relaxation time scale of $\tau = 3600$ s. *Reed et al*. [2012] suggested that using an 1800 s physics time step produced more realistic tropical cyclone intensities by providing more reasonable partitioning between the large-scale and convective precipitation in CAM. Cold ice and rain water autoconversion coefficients were set to match the defaults for high-resolution (0.25°) CAM-FV runs. All other physical parameterization tuning parameters are CAM defaults which are derived from 1° CAM-FV simulations documented in *Neale et al*. [2010].

In the variable-resolution simulation, topography is differentially smoothed by starting with an initial high-resolution data set and applying a Laplacian smoother over the global domain. The smoothing is scaled approximately by element area as in the hyperdiffusion formulation, providing more (less) smoothing over areas tiled with larger (smaller) elements. The newly smoothed data provide conservatively mapped values for subgrid variability of topography needed for the parameterization of turbulent mountain stress, subgrid orographic drag, and momentum flux deposition due to gravity waves [*Lauritzen et al*., 2012]. The overall magnitude of the smoothing is constrained such that it closely matches the profile of the operational default topography data used for uniform-resolution simulations in CESM. To lessen atmospheric noise with rougher topography at higher resolution, CAM-SE typically applies enhanced damping of divergent motion within the momentum equations at 0.25° [*Lauritzen et al*., 2014]. However, given the findings of *Zhao et al*. [2012] which showed potentially significant sensitivity of GCM-simulated TCs to a divergence damping mechanism, we have chosen to utilize a slightly smoother topography profile in the high-resolution nest such that numerical noise near topographical peaks is eliminated. Therefore, the hyperdiffusion coefficient (Table 1) is identical for both the rotational and divergent flow components.

The simulations follow AMIP protocols. SSTs are specified by the Hadley Centre Sea Ice and Sea Surface Temperature data set [HadISST, *Hurrell et al*., 2008]. Greenhouse gas concentrations and aerosol climatology are also prescribed to reproduce past observations. Both simulations are initialized in September 1979, although the first 4 months are discarded for model spin-up. Both experiments are integrated through the middle of 2003, although only the years 1980 through 2002 (inclusive) are analyzed in this manuscript. The variable-resolution model run was conducted on NCAR's Bluefire machine (IBM POWER6 processors) and

averaged ~0.42 simulated years per day on 384 cores. The 1° simulation was completed on the Agri computing cluster (Intel Xeon processors) at the University of California, Davis. Due to the coarse grid having fewer elements and a longer time step, model throughput was ~2.5 simulated years per day on 384 processors, although a direct comparison of simulations across different hardware platforms is difficult.

3. Tropical Cyclone Detection Algorithm

Objective detection of tropical cyclones within the climate data set was performed using a method similar to that described in *Vitart et al.* [1997] and *Knutson et al.* [2007]. Candidate cyclones were detected in 6 hourly model output as follows:

1. All local 850 hPa vorticity maxima greater than 1.0×10^{-4} s^{-1} at 850 hPa were found between the latitudes of 45°S and 45°N.
2. For each maximum, the nearest collocated sea level pressure (SLP) minimum was defined as the storm center. This minimum must occur within 4° of the 850 hPa vorticity maximum.
3. The nearest local maximum of 500–200 hPa average temperature is defined as the center of the warm core. This cannot be offset from the storm center by more than 2°. From the center of the warm core, the temperature must decrease by at least 0.8 K out to 5° in all directions.

An allowable 4° offset between the SLP minimum and 850 hPa vorticity maximum [compared to 2° in *Knutson et al.*, 2007] was found to provide fewer "misses" of weaker or broader storms which sometimes contained multiple vorticity peaks or elongated pressure minima within the circulation. It also assisted in alleviating the occasional double counting of broken trajectories as discussed in *Camargo and Zebiak* [2002].

The 850 hPa vorticity field is calculated from the zonal and meridional wind components using spherical harmonics. A nine-point filter was used to apply localized smoothing of the vorticity field and damp grid-scale maxima that may influence the tracking algorithm, especially when tropical cyclones are near areas of steep topography (e.g., Bay of Campeche, Yucatan Basin). Unlike past studies using lower resolution data [e.g., *Vitart et al.*, 1997], splines were not used to interpolate between grid cells so as to not introduce overshoots or undershoots beyond the model resolution's capability. Simple tests comparing splined and non-splined fields showed negligible difference in detected storms and avoiding extraneous interpolation greatly sped up the tracker's computational runtime.

Once candidate tropical cyclones were collected using the above criteria, trajectories were computed as follows:

1. Search for storms that occur within 400 km the following 6 h period (this translates to an average forward velocity of 18.5 m s^{-1} or 41.4 mph).
2. If no storms exist with the above criteria, the trajectory of a detected storm is considered terminated. If only one storm is detected within 400 km, it is considered to be the same storm. If multiple storms occur within the 400 km region, first preference is given to storms in the northwest quadrant (Northern Hemisphere) or southwestern quadrant (Southern Hemisphere) and the closest storm is chosen as belonging to the same trajectory as the initial storm from the previous 6 h period.
3. The maximum surface wind velocity within 4° of the storm center must be greater than 17 m s^{-1}. To be considered a full trajectory, the storm must persist for at least 2 days. These days do not have to be consecutive.

This setup allows for the candidate cyclone algorithm to be embarrassingly parallel on parallel computing architectures. The model data can be broken up into an arbitrary number of subsets and candidate cyclones are detected in parallel. Following the completion of this process, the list of possible cyclones is sorted and consolidated before trajectories are determined.

To further eliminate broken tracks, storms originating within 12 h and 400 km of a previous storm's termination point are merged with the previous storm. These merged systems tend to be weak, but long-lived, storms which fail to satisfy the candidate cyclone criteria during intermittent 6 h intervals. They occurred

Table 2. Saffir-Simpson (S-S) Intensity Scale

	Wind Speed			
S-S Category	m s^{-1}	knots	mph	km h^{-1}
Tropical depression	<17	<34	<38	<62
Tropical storm	18–32	35–63	39–73	63–118
Category 1	33–42	64–82	74–95	119–153
Category 2	43–49	83–95	96–110	154–177
Category 3	50–58	96–112	111–129	178–208
Category 4	58–70	113–136	130–156	209–251
Category 5	≥70	≥137	≥157	≥252

only once globally approximately every 5 years in the model data, highlighting the robustness of the tracker.

The surface wind is calculated by taking the wind at the center of the model's lowest level (approximately 60 m) and correcting it to 10 m using a logarithmic law with an open sea roughness coefficient [*Garratt*, 1992; *Wieringa*, 1992]. Logarithmic profiles have been shown to approximate below-maximum winds in tropical cyclones [*Giammanco et al*., 2012]. This correction results in approximately a 15% reduction in wind speed between the lowest model level and 10 m.

We compare the model results to observational data. For historical tropical cyclone climatology, we use the International Best Track Archive for Climate Stewardship (IBTrACS) tropical cyclone best track database [*Knapp et al*., 2010]. All observed wind speeds are corrected to 1 min averages using the methodology outlined in *Harper et al*. [2010]. This is done to homogenize wind speed observations, although no correction is required for the Atlantic and East Pacific, where the National Hurricane Center is the primary source of cyclone data. The Saffir-Simpson scale [*Simpson*, 1974] is used to simplify intensity analysis although we note that the model winds are defined as instantaneous as opposed to 1 min averages. The categories within the Saffir-Simpson scale are outlined in Table 2 along with corresponding surface wind speed thresholds. Since our focus is primarily on the North Atlantic basin, we use the term "hurricane" to represent any storm with wind speeds greater than 33 m s^{-1}. The term "major hurricane" signifies a storm that equals or exceeds category 3 on the Saffir-Simpson scale (≥50 m s^{-1}). For all other analysis of the large-scale environment, we use the NCEP/NCAR Reanalysis [*Kalnay et al*., 1996].

4. Results

4.1. Spatial Patterns of Storm Origins and Trajectories

Figure 2a displays color-coded trajectories of all tropical cyclones in the simulation with the globally uniform 1° mesh. Data from all 23 years are shown. When compared to observations (Figure 2c), the model does an adequate job of producing TCs in climatologically active locations. However, the low resolution of the model precludes simulation of the correct spatial pattern and density of storms in all ocean basins. In particular, with the uniform 1° grid spacing, TC development is deficient in the North Atlantic, East Pacific, and West Pacific, with the model simulating only a fraction of observed TCs.

TC trajectories in the variable-resolution simulation are plotted in Figure 2b. The high-resolution patch lies within the innermost black outline. The transition band (0.5°) lies between the two black grid outlines. The resolution outside the outermost black contour matches the coarse 1° simulation in Figure 2a. In the North Atlantic, TC density increases greatly and becomes much more similar to observations. In addition to the increased number of storms, more intense storms, represented by warmer colors, are better represented. Where the coarse simulation could only support the occasional tropical cyclone which reached category 1 strength, the variable-resolution run contained multiple storms which are classified as "major storms" (category 3 and higher) on the Saffir-Simpson scale.

An increase in storm count is seen in the East Pacific within the variable-resolution simulation as well. This is attributable to the 0.5° transition region between the 0.25° nest over the Atlantic and the remainder of the global domain. It is worth noting that the number of storms increased, but the intensities remained relatively weak, implying that while 0.5° in CAM is more amenable to TC genesis, it remains unsuitable for simulating particularly intense cyclones. The remainder of the global basins, such as the Western Pacific, Southern Pacific, and Indian Oceans appear very similar in Figures 2a and 2b. This highlights that the TC deficiency due to the 1° grid spacing exists regardless of which simulation is analyzed.

Storm origin locations in the North Atlantic basin are shown in Figure 3 for both CAM-SE simulations as well as observations. The color denotes the maximum intensity each tropical cyclone reaches during its lifetime.

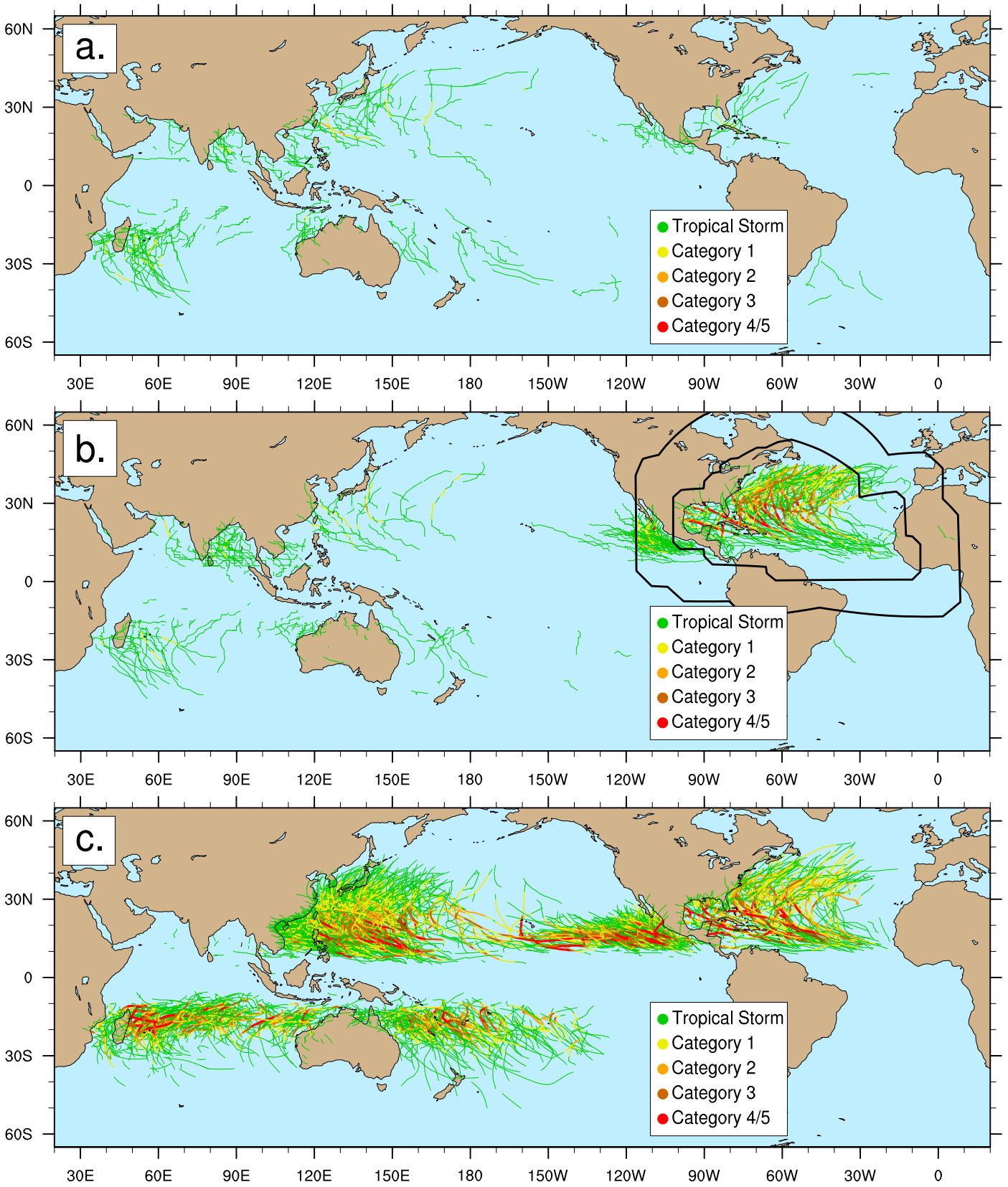

Figure 2. Global distribution of storm trajectories from 1980 to 2002 in the (a) global 1° simulation, (b) variable-resolution simulation, and (c) IBTrACS observational data set. Storm paths are color coded by intensity at each location in their trajectory. The outline of the high-resolution nest is shown in black in Figure 2b.

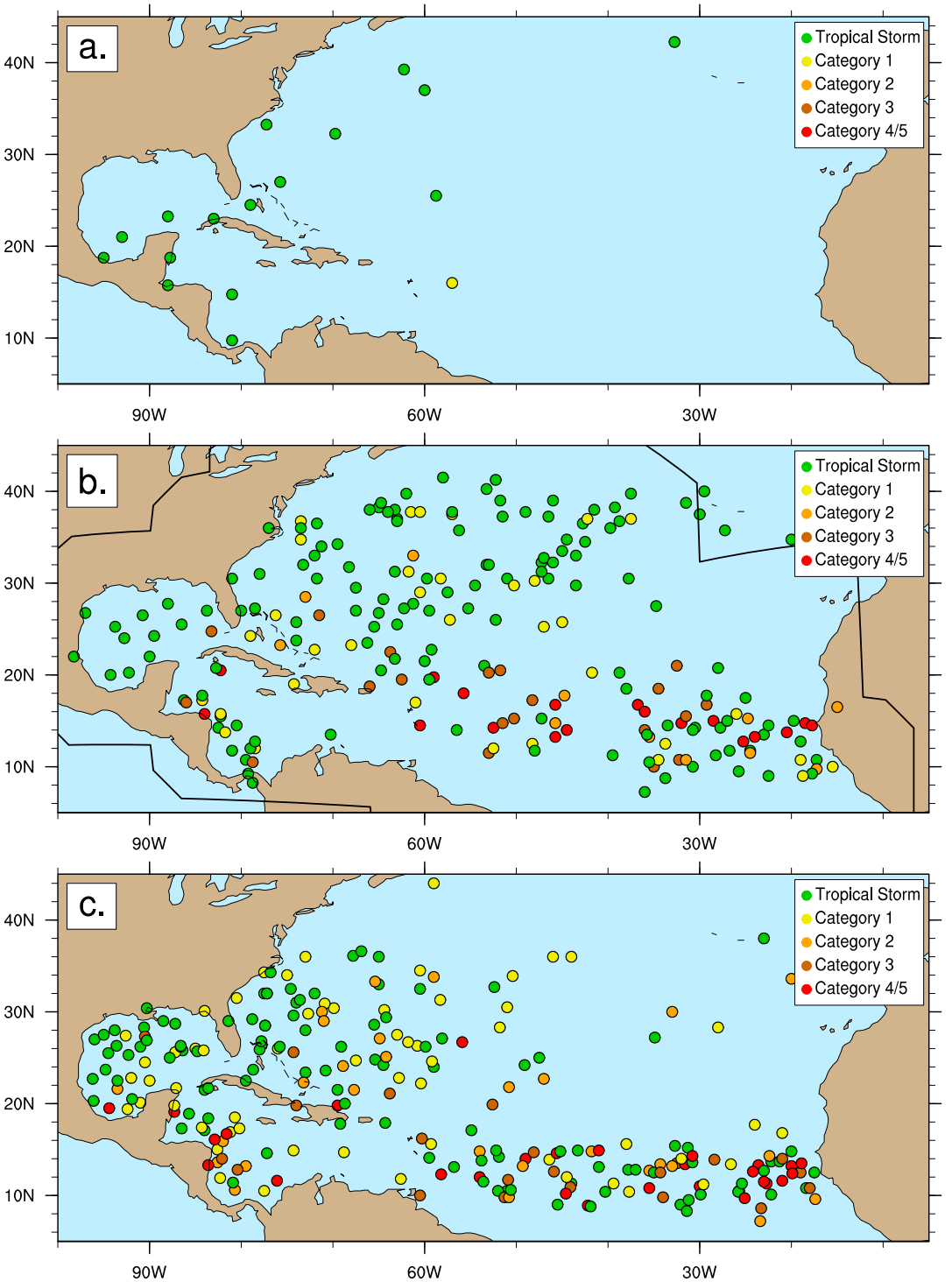

Figure 3. TC genesis locations from 1980 to 2002 in the (a) global 1° simulation, (b) variable-resolution simulation, and (c) IBTrACS observational data set. Storms are color coded by peak intensity during their lifetime. The outline of the high-resolution nest is shown in black in Figure 3b.

Figure 3a again shows that very few storms are supported by the 1° grid spacing, with the majority forming over the western half of the basin. A much more realistic distribution of genesis locations is seen in the variable-resolution run (Figure 3b) when compared to observations (Figure 3c). In particular, genesis occurs further east, with storms forming just off the African coast and across the Main Development Region (MDR),

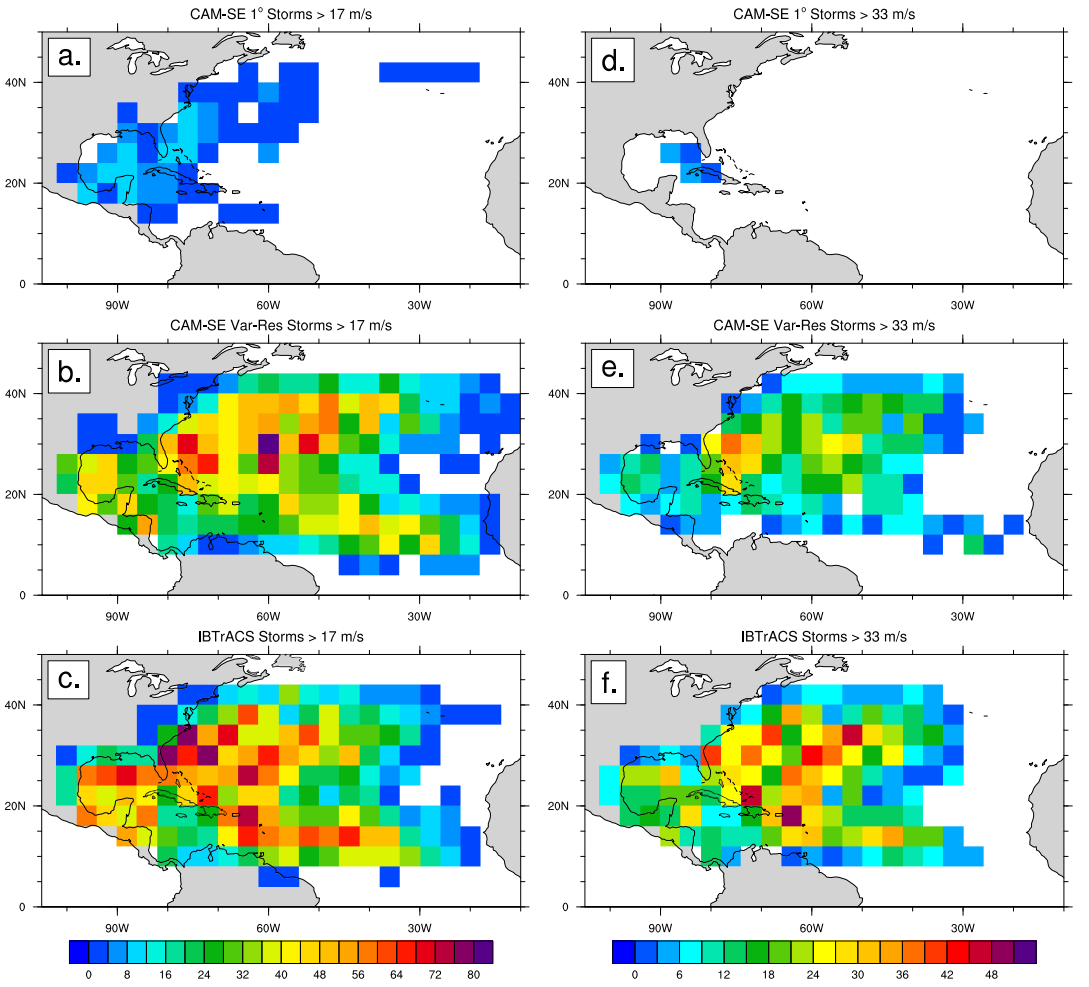

Figure 4. Track density plots for North Atlantic (left) all tropical cyclones (>17 m s^{-1}) and (right) hurricanes (>33 m s^{-1}) in global coarse (1°, top) and variable-resolution (0.25°, middle) simulations as well as observations (bottom). Units are cumulative 6 hourly storm position frequency per 4° × 4° gridbox for the period 1980–2002.

the area of the Atlantic bounded by 10–20°N and 20–85°W. The var-res simulation is able to adequately capture the genesis of Cape Verde storms. In addition, the majority of the simulation's intense (category 3 or greater) storms form in this region, similar to observed data. The model also reproduces the local minimum in TC genesis over the eastern Caribbean Sea as well as the local maximum over the Gulf of Honduras and the southwestern Caribbean. Over the Gulf of Mexico, the model only produces approximately 50% of the observed TC formation rate, and those storms that form are weaker. While the majority of Gulf of Mexico storms in the IBTrACS data also only attain tropical storm status, occasional storms intensify into hurricanes or major hurricanes, a feature not simulated by CAM-SE. Additionally, the model generates too many weak storms north of 35°N. This may be a result of the tracking algorithm and is discussed more in depth in section 4.5.

Figures 4a–4c show the Atlantic track densities for all TCs during the 1980–2002 time period for both model simulations (a,b) and observations (c). Each 6 h latitude-longitude pair for tracked tropical cyclones between 1980 and 2002 is binned into 4° × 4° gridboxes. Again, it is evident that the coarse simulation (Figure 4a) is highly deficient in simulating TCs. TCs that do form do not follow a coherent pattern of tracks that mimic observations (Figure 4c). The var-res simulation (Figure 4b), however, exhibits a pattern of cyclone tracks that is much more correlated with observations. Cape Verde trajectories originating in the eastern half of the basin are apparent as well as the general recurvature pattern that occurs with the majority of Atlantic TCs. In addition, the var-res simulation simulates the dual peaks in the center of the ocean basin, with one lying just off the coast of the southeastern United States and the other in the central Atlantic.

Table 3. TC Statistics (Counts) for Coarse 1° Simulation (Left), Var-res Simulation (Middle), and IBTrACS Observations (Right)[a]

	Uni. 1°			Var-res			Obs.		
	NATL	EPAC	GLOB	NATL	EPAC	GLOB	NATL	EPAC	GLOB
Resolution	1°	1°	1°	0.25°	0.5°	1°			
TC	0.7 (0.8)	0.7 (0.8)	9.0 (3.4)	9.6 (3.4)	4.8 (1.9)	7.9 (2.9)	10.7 (3.6)	16.0 (4.1)	77.3 (8.1)
Hurr	0.0 (0.2)	0.0 (0.0)	1.0 (1.0)	3.6 (2.5)	1.1 (0.8)	0.8 (0.8)	6.0 (2.6)	9.2 (2.8)	32.4 (4.9)
MH	0.0 (0.0)	0.0 (0.0)	0.0 (0.0)	1.6 (1.6)	0.1 (0.3)	0.0 (0.0)	2.2 (1.6)	4.6 (2.3)	14.3 (4.1)
TC days	2.3 (2.6)	1.9 (2.8)	30.6 (12.9)	48.4 (24.2)	18.3 (7.8)	27.3 (11.6)	51.8 (26.0)	75.1 (26.9)	308.2 (56.4)
Hurr days	0.1 (0.5)	0.0 (0.0)	1.2 (2.2)	13.4 (11.1)	1.8 (2.3)	1.2 (1.4)	22.6 (15.9)	32.2 (13.6)	116.0 (31.7)
MH days	0.0 (0.0)	0.0 (0.0)	0.0 (0.0)	3.7 (4.0)	0.0 (0.1)	0.0 (0.0)	4.6 (4.5)	9.8 (5.8)	27.8 (11.9)
ACE	2.0 (2.7)	1.4 (2.3)	25.0 (12.3)	72.0 (48.1)	16.5 (9.0)	22.0 (10.6)	91.3 (58.3)	139.3 (59.1)	525.1 (125.8)

[a]Categories are TC (all storms tropical storm strength or greater), Hurr (only hurricanes), MH (only major hurricanes), and accumulated cyclone energy (ACE). The standard deviation is denoted in parentheses.

Figures 4d–4f show the same analysis with only storms of hurricane strength or higher considered. The global 1° simulation (Figure 4d) is nearly devoid of all hurricane formation whereas the var-res simulation (Figure 4e) produces a more robust signature similar to observations (Figure 4f). The var-res simulation continues to show the double peak in the track densities over the central Atlantic but is biased low over the entire basin. As implied from the cyclone origins, this bias is especially prevalent over the Gulf of Mexico. This underprediction of storms in the Caribbean and Gulf of Mexico has been observed in other high-resolution climate models [*Strazzo et al*., 2013] and may impact regional analysis of landfalling TCs in the southeastern United States. In addition, the var-res simulation has lower track densities over the eastern Atlantic. When assessed together with Figure 4b, the var-res simulation produces a realistic count of Cape Verde storms, but these storms strengthen to hurricanes more slowly and less frequently than their observed counterparts, leading to this low bias in hurricane density stretching over much of the low-latitude Atlantic.

4.2. Annual Average Statistics

Annual cyclone statistics (counts) averaged over the 1980–2002 period are shown in Table 3. Results are shown for the 1° coarse run (left), variable-resolution simulation (middle), and observations (right). Each model is broken out into three spatial subsets shown in Figure 5. These subregions (North Atlantic (NATL), East Pacific (EPAC), and "rest of globe" (GLOB)) represent the three different resolutions (0.25°, 0.5°, and 1°) in the variable-resolution simulation. We use the standard deviation of the statistical time series as a proxy for the measure of interannual variability (in parentheses).

When compared to the coarse grid, the number of TCs generated by the variable-resolution simulation in the North Atlantic (9.6 per year) is very similar to IBTrACS observations (10.7 per year). While the model simulation only simulates 60% of the observed hurricane count, it produces 1.6 major hurricanes per year (category 3 strength or higher), compared to 2.2 in observations. TC, hurricane, and major hurricane days (cumulative summation of the lifetimes of all storms during a given calendar year) all show similar results when comparing the North Atlantic in the var-res simulation to observations. The fact that storm counts and storm days share the same proportional biases shows that lifetimes of individual storms are well represented in the model.

Accumulated Cyclone Energy (ACE) is an integrated measure of TC activity which combines intensity and duration [*Bell et al*., 2000]. ACE is defined as

$$\mathrm{ACE} = 10^{-4} \sum v_{max}^2 \tag{1}$$

where v_{max} is the maximum surface wind (in knots) for the TC at a given time. The sum is taken over all 6 hourly observations during a TC's lifetime. ACE from individual TCs can be summed regionally (over a calendar year, for example) to produce basin-wide statistics. The simulated annual mean ACE in the North Atlantic is ~79% of the observed mean due to the low bias in the number of hurricane strength TCs. The standard deviations of all NATL statistics are also in good agreement with observations which shows that year-to-year variability in storm genesis is well simulated.

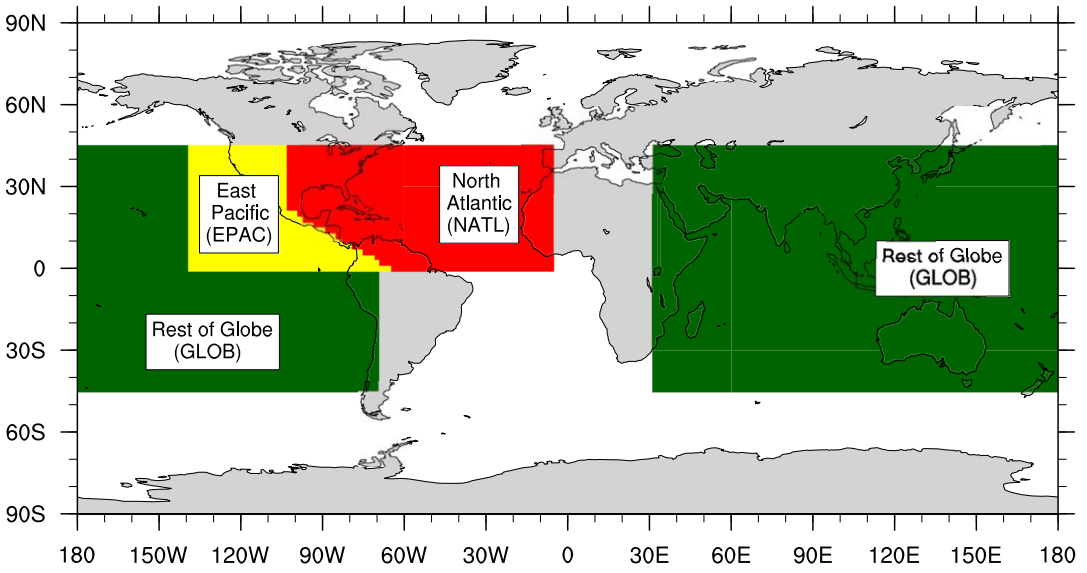

Figure 5. Basin mask definitions used for calculating TC statistics.

Storm counts are biased low in the Eastern Pacific within the variable-resolution simulation. With the basin lying in the 0.5° transition region between the high-resolution North Atlantic nest and the global 1° base mesh, it produces TC statistics that lie between the coarse, 1° simulation and observations. The var-res model produces 4.8 TCs/year, ∼30% of the observed count. It only produces ∼12% of the observed hurricanes, however (1.1 hurricanes/year compared to 2.9), further indication that the 0.5° grid spacing struggles to sustain more intense cyclones. This is also highlighted by the fact that the simulated ACE in the East Pacific of the var-res simulation is also only ∼12% of the observed average.

In all ocean basins, the coarse simulation produces very few TCs and only approximately one storm of hurricane strength or greater per year at the global scale. No storms with intensity greater than category 3 develop and simulated ACE is between 1 and 4% of the observed value. These results emphasize the inadequacy of coarser model grid spacings to generate and sustain realistic tropical cyclones within a long-term climate simulation.

A positive result is that the GLOB statistics are nearly identical between the coarse 1° simulation and the variable-resolution run. These storms are simulated at the same grid resolution, so their similar statistics are a good indication that the model result in the 1° portion of the variable-resolution simulation closely matches the climatology of the globally uniform 1° simulation without refinement.

4.3. Resolution Impact on Intensity

Figure 6 shows the average number of TCs per year which reached each Saffir-Simpson category for the variable-resolution simulation (Figures 6a–6c) and in observations (Figures 6d–6f) during the 1980–2002 period. Note that the total count is scaled differently in Figure 6f. In the Atlantic basin (Figure 6a), we see that the majority of storms tracked in the simulation are tropical storms. This is similar to the observed distribution (Figure 6d) although the total number of storms only reaching tropical storm strength is higher in the model (6 per year) than observations (4.7 per year). The overall shape of the modeled distribution is similar to observations. The modeled intensities are biased low, with the relative fraction of hurricanes greater than category 1 intensity being lower than observed. However, the model still generates between 1 and 2 major hurricanes (category 3 or higher) per year.

In the Eastern Pacific, the negative intensity bias in the model (Figure 6b) is more apparent and evidenced by a shift in the distribution left (toward weaker storms). This is due to the fact that the majority of the Eastern Pacific basin is simulated at 0.5° equivalent grid spacing. When compared to observed intensities (Figure 6e), very few cyclones greater that category 1 intensity occur, although there is one instance of a category 4 strength cyclone. However, while the intensity is biased low, the absolute count of modeled

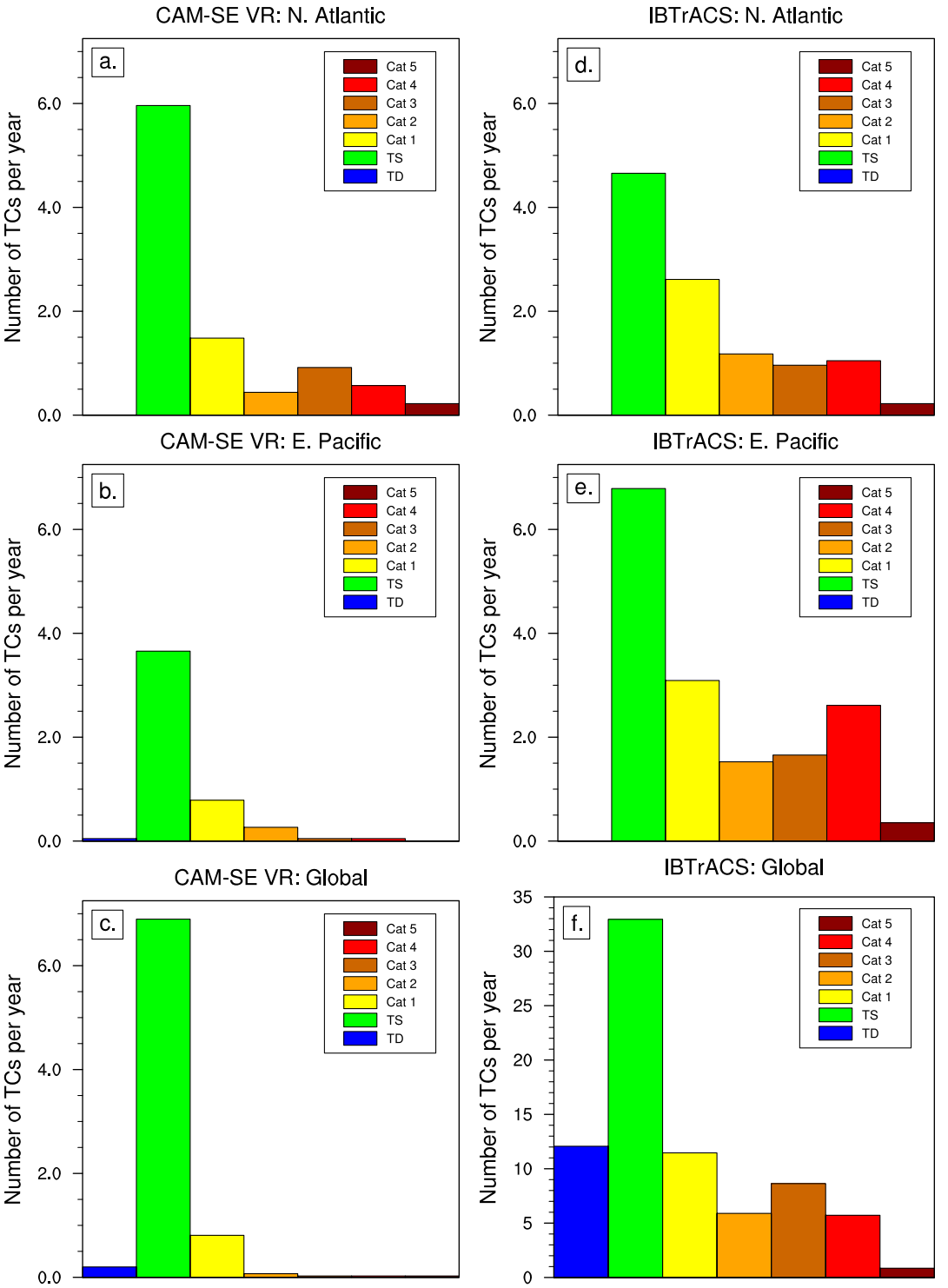

Figure 6. Annual storm count (averaged over 23 years) binned by maximum Saffir-Simpson intensity (color) and basin for the variable-resolution (VR) simulation (left) and observations (right). The equivalent VR model resolution for the (top) North Atlantic basin is 0.25°, (middle) East Pacific is 0.5°, and (bottom) rest of the globe is 1°. Note the difference in the y-axis in plot (f).

tropical storms remains on the same order of magnitude as observations. All storms in basins other than the Atlantic and Eastern Pacific (rest of globe) are shown in Figures 6c (var-res model) and 6f (observations). At 1° grid spacing, the model struggles to simulate any storms beyond tropical storm strength. The scale of

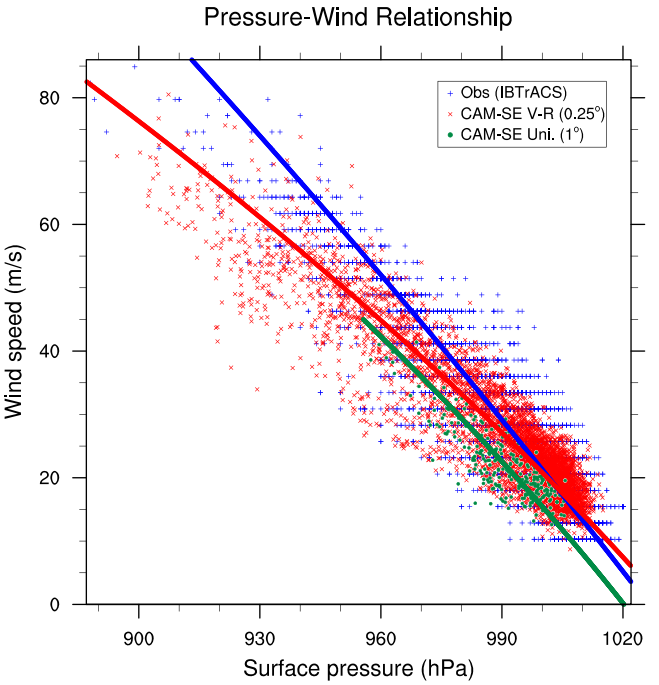

Figure 7. Pressure-wind pairs for each 6 hourly TC measurement for (green) global 1° simulation, (red) variable-resolution simulation, and (blue) observations. Surface (10 m) wind is used. A quadratic regression is fit to each distribution of pressure-wind pairs.

the y-axis is approximately a factor of 5 less than that used for the observations, underscoring the model's ability to only resolve a fraction of the annual number of TCs in the 1° part of the mesh.

The pressure-wind curve for the Atlantic Basin is plotted in Figure 7 and follows the analysis of *Atkinson and Holliday* [1977]. Each individual 6 hourly surface pressure −10 m (surface) wind pair is plotted for the variable-resolution simulation (red, x's), the coarse 1° simulation (green, dots), and observations (blue, crosses). A quadratic fit is regressed to the data and overlaid as a solid line. The fit for the coarse simulation is truncated at 45 m s^{-1} due to the nonexistence of stronger storms in the data. The coarse simulation pressure-wind pairs fall within the envelope of that from the var-res model, implying that the CAM5 physical parameterizations governing the intensity relationships within weaker tropical cyclones behave similarly at both 0.25° and 1°. The 0.25° North Atlantic grid is well matched to observations in terms of spread and extent of the pressure-wind relationship. The model is able to produce multiple storms with minimum central pressures deeper than 930 hPa and maximum surface winds greater than 60 m s^{-1}. These results are well matched to a similar analysis of storms in a 0.25° CAM-FV simulation using identical prescribed SST and ice data (Wehner et al., submitted manuscript, 2014).

There is a downward bias in the best fit curve relative to wind speed. While the model adequately produces the overall spread seen in observations, extreme (low) surface pressures do not produce wind speeds high enough to match observations. This is especially prevalent at surface pressures lower than 960 hPa. This is a similar result to previously published model-derived pressure-wind curves [*Oouchi et al.*, 2006; *Knutson et al.*, 2007; *Manganello et al.*, 2012; *Satoh et al.*, 2012]. *Manganello et al.* [2012] proposes that this deficiency may arise due to the lack of explicitly resolved convection as well as unrealistic surface roughness parameterizations in the most intense storms. It is worth noting that inconsistencies in the historical record have been highlighted recently [*Knaff and Zehr*, 2007]. In addition, the pressure-wind relationship is highly sensitive to the manner in which surface winds are derived in model output, so future work standardizing how tropical cyclone intensity is assessed within climate models may be useful in addressing some of these issues.

4.4. Resolution Impact on Storm Structure

Figure 8 is a four-plot snapshot of the most intense storm generated in the var-res simulation. The storm formed in the high-resolution nest over the Atlantic Ocean in August 1985. It developed in the MDR before tracking north of the Caribbean and into the Gulf of Mexico. The storm reached a maximum surface wind intensity of 80 m s^{-1} (minimum surface pressure of 895 hPa). Figure 8a shows the instantaneous horizontal 850 hPa wind at the storm's peak intensity. The storm exhibits a classical, intense tropical cyclone structure [*Frank*, 1977]. This includes a calm eye, strong winds located in a tight eyewall, and a local wind maximum in the northeast quadrant due to the storm's northwesterly motion. The simulated radar reflectivity at the same instant is shown in Figure 8b. Spiral rainbands are evident, as well as an intense area of precipitation under the central dense overcast (CDO). A minimum in precipitation in the area of the storm's eye is also apparent. Figures 8c and 8d show the longitude-height cross sections of the wind speed and temperature anomaly, respectively. The temperature anomaly is calculated by subtracting an environmental reference

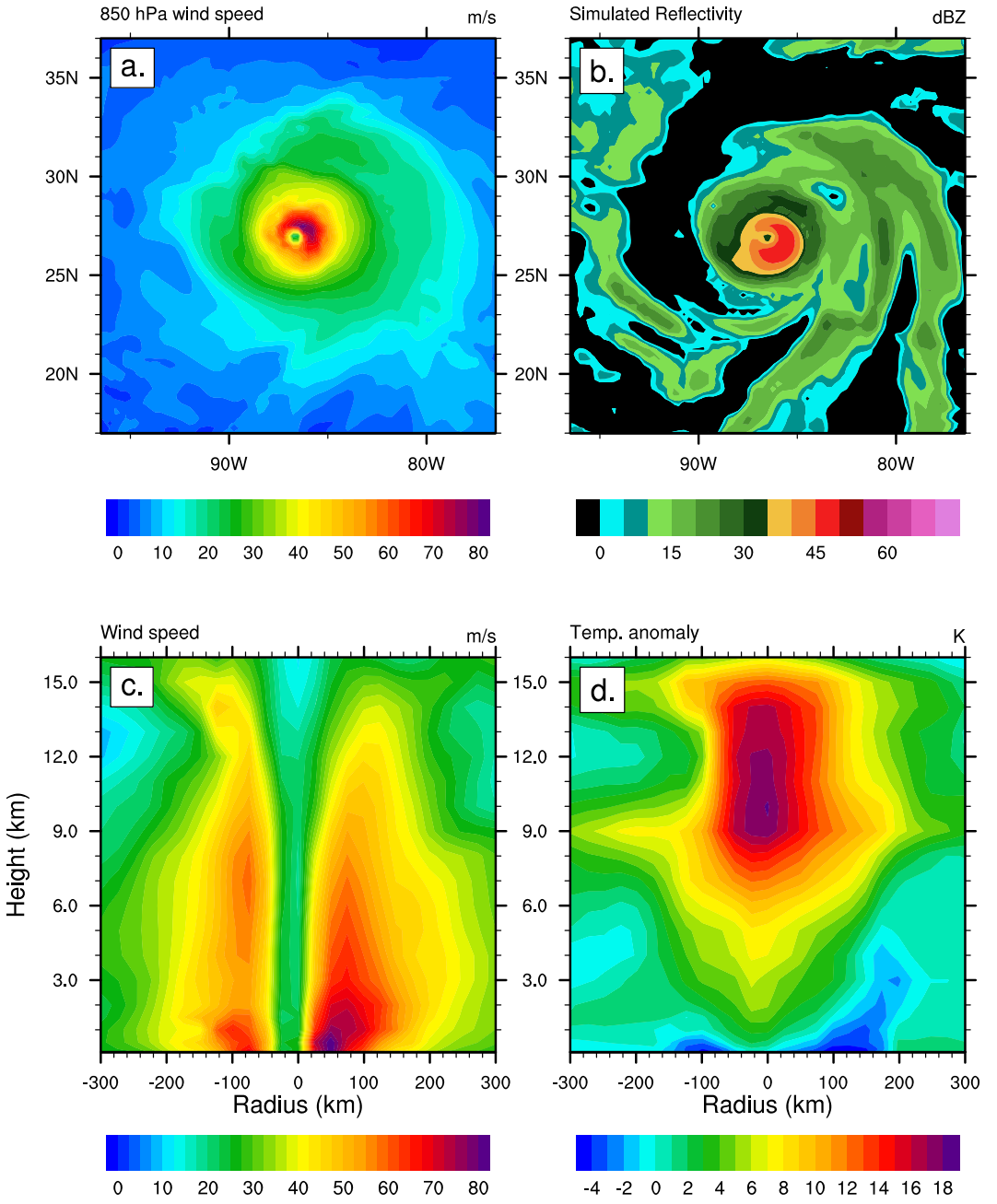

Figure 8. (a) 850 hPa horizontal wind, (b) simulated radar reflectivity and (c) longitude-height cross sections of the horizontal wind speed and (d) temperature anomaly for the most intense storm generated in 0.25° (North Atlantic) mesh. The radius measures distance to the center of the storm as defined by the surface pressure minimum.

temperature profile taken from approximately 350 km from the cyclone center along the same latitude. The cyclone exhibits a calm eye at all levels and a low-level wind maximum. An outward slope in the wind contours with height matches observations of intense TCs [*Hazelton and Hart*, 2012]. In addition, a strong warm core associated with diabatic heat release is located between 9 and 12 km above the cyclone center.

Figure 9 is the same as Figure 8 except for one of the most intense storms that developed in the North Atlantic in the coarse simulation (1°). The storm also formed in the MDR in August 1989. It reached a maximum wind speed of 31 m s^{-1} and a minimum pressure of 973 hPa. When compared to the Atlantic storm depicted in Figure 8, the coarse grid storm shows a much broader and weaker wind field (Figure 9a). There are no inflow bands in Figure 9b. In addition, while the CDO is evident, it is weaker and does not

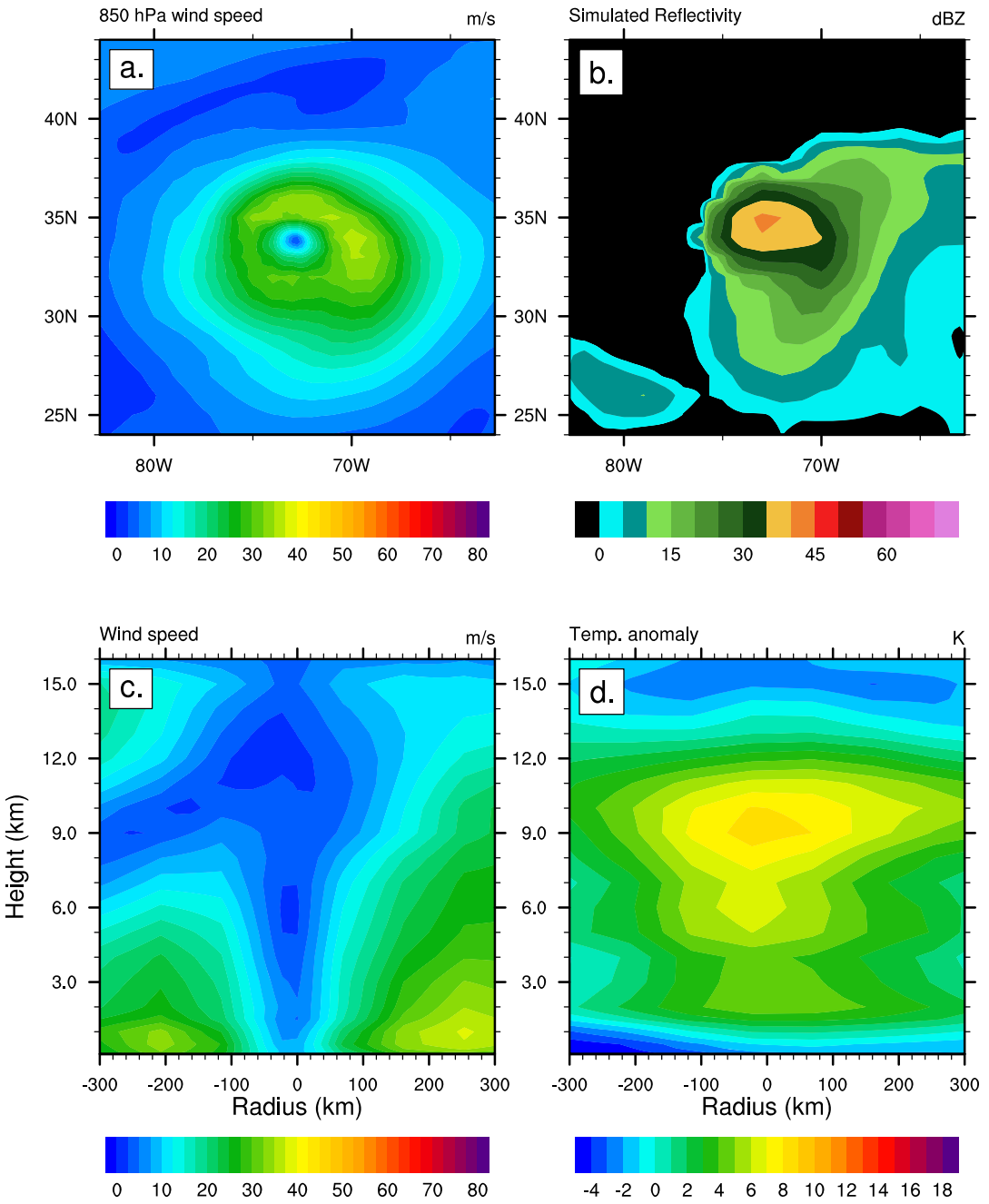

Figure 9. Same as Figure 8 but for a North Atlantic storm generated in 1° simulation.

have a readily apparent eye, even though a local wind maximum is discernible at the center of the cyclone in Figure 9a. Figures 9c and 9d show that the coarse grid storm is much weaker and less similar to intense tropical cyclones seen in observations. The storm exhibits a broader, shallower wind field as well as a lower, much more diffuse warm core. While only snapshots of individual storms within the model simulation, these results highlight the differences in dynamical storm structure between the two grid spacings.

4.5. Reproducibility of Seasonal Cycle

The seasonal cycle of TC genesis in the North Atlantic is plotted in Figure 10. TC count by month is plotted in Figures 10a–10c for the var-res simulation and observations. Note that these use different y-axis scales to

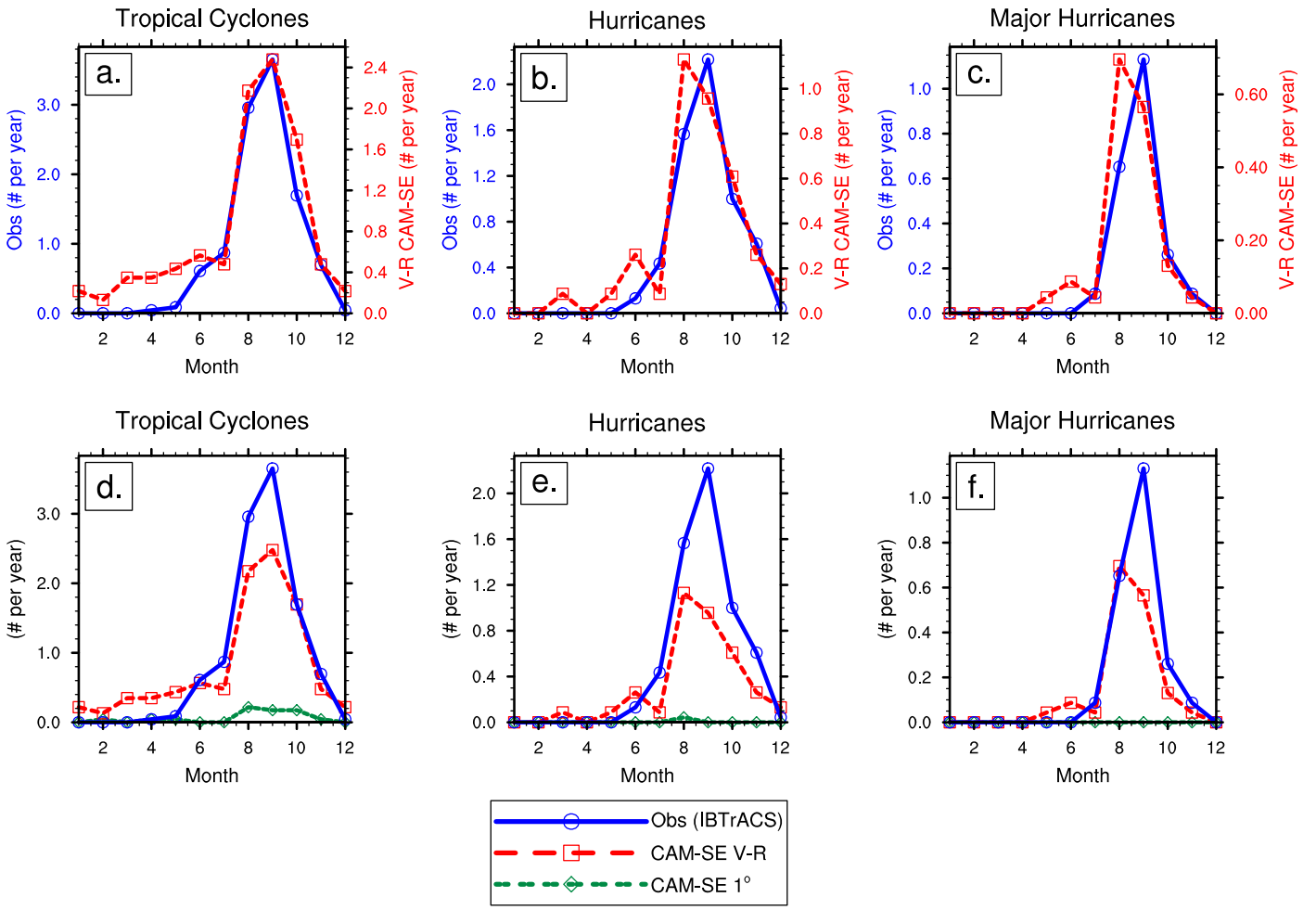

Figure 10. Average annual cycle of (left) TC, (middle) hurricane, and (right) major hurricane formation rates. (a–c) Comparison between (red, right y-axis) the var-res model and (blue, left y-axis) observations and are normalized using separate axes. (d–f) Storm formation rates on the same scale and also include the 1° coarse simulation (dark green). The calendar month (in numeric format) is labeled on the x-axis in all figures.

emphasize the overall shape of the distribution. The model (red) reproduces the correct observed (blue) peak for all TCs (Figure 10a) with September being the most active month, followed by August, and then October. When only storms of hurricane strength or stronger are considered (Figure 10b), the model's peak is shifted 1 month early relative to observations. The same trend holds true for major TCs (Figure 10c). Figures 10d–10f display the counts for all TCs, hurricanes, and major hurricanes in the Atlantic on the same scale. The 1° simulation is shown in green. We see that the var-res model slightly underpredicts the peak number of storms at all intensity scales, in agreement with the results from section 4.2. The 1° simulation shows approximately the correct peak in activity from a temporal standpoint but produces fewer than one TC per year.

We note that the tracker detects a few weak storms during months outside the Atlantic hurricane season (January–May) (Figures 10a and 10d). Subtropical storms (cyclones with hybrid tropical and extratropical characteristics) remain a gray area between purely warm or purely cold-core systems, with questions as to how well they are demarcated from tropical cyclones in models, the historical record, or even current observations [*Guishard et al.*, 2009]. A cursory analysis of some of the detected storms indicates that approximately one or two storms per ocean basin per year may be subtropical or warm-seclusion extratropical cyclones. These storms generally occur off-season and at higher latitude. *Knutson et al.* [2007] found likewise biased storm counts in the northern North Atlantic using a similar tracking technique. A manual classification of all tracked storms is beyond the scope of this project. However, these biases are relatively low compared to overall TC count.

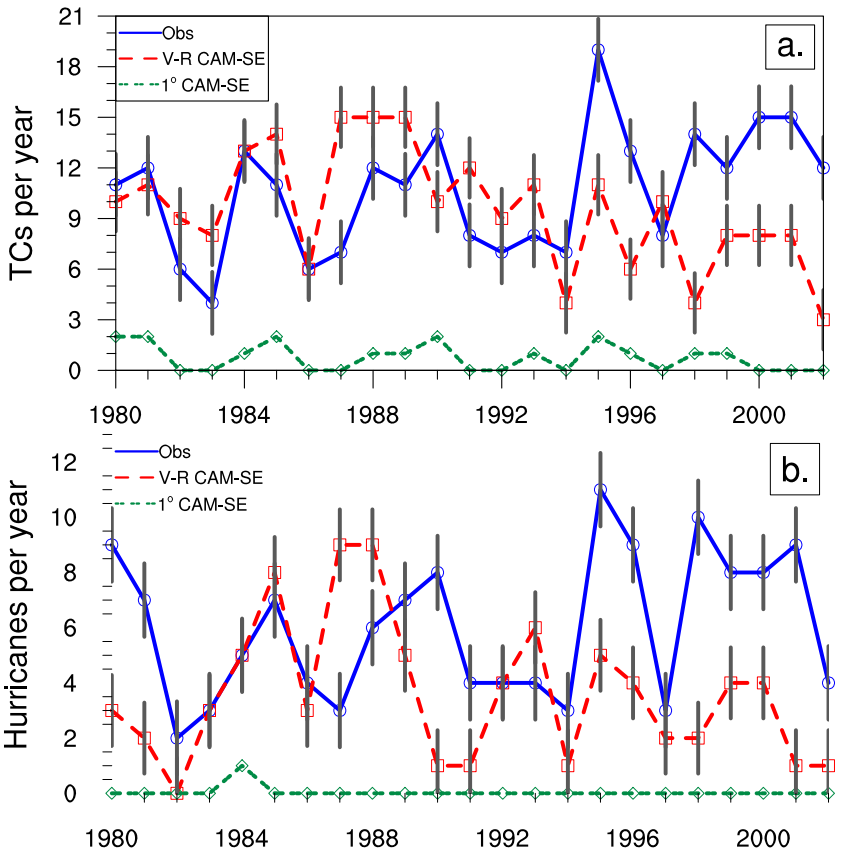

Figure 11. Number of (a) tropical cyclones and (b) storms which reach hurricane strength as a function of calendar year for the var-res (red) and global 1° models (green) as well as observations (blue). Gray, vertical lines show standard deviations of interannual storm counts.

4.6. Interannual Variability

4.6.1. Interannual *Storm Activity*

Simulated TCs as a function of calendar year are plotted in Figure 11. Figure 11a shows all storms tracked throughout the model integration for both the variable-resolution simulation (red) and the global coarse simulation (green). Observations are shown in blue. The model does not reproduce the slight increase in cyclone counts over the 1980–2002 time period, and, in fact, exhibits a slight decrease. Certain features, such as the local maximum in TC activity in 1984–1985 and the decline in storm counts from 1990 to 1994 are well matched between var-res simulation and observations. However, other aspects, like the spike in 1995 are not well captured. The 1° simulation appears to approximate "active" or "not active" seasons but fails to generate more than two storms in any given season. The number of storms which reach hurricane strength is plotted in Figure 11b, with similar results to those seen in Figure 11a.

To quantify the ability of CAM-SE to reproduce the proper change in sign in overall cyclone activity between seasons, both the historical and CAM time series plotted in Figure 11 are first linearly detrended. There remains question as to whether the upward trend in cyclone count between the 1980s and the mid-2000s was, in part, due to advent of new observing techniques such as wind scatterometers and better satellite measurements [*Landsea et al.*, 2009]. The correlation between model and observations for the detrended yearly TC counts in the North Atlantic is 0.28 and 0.23 for ACE. The correlation for TCs is similar to that found in single-simulation studies such as *Bengtsson et al.* [2007], *Murakami et al.* [2012] and Wehner et al. (submitted manuscript, 2014) but lower than the ensemble simulations of *LaRow et al.* [2008], *Zhao et al.* [2009], and *Strachan et al.* [2013]. This result may highlight the need for ensemble simulations to increase confidence in modeled TC statistics, especially given the relatively low frequency and chaotic nature of TC genesis over short time periods.

Correlation coefficients for modeled versus observed hurricanes, tropical cyclone days, and hurricane days are also all positive (between 0.10 and 0.25), indicating some potential skill, but the correlation fails to

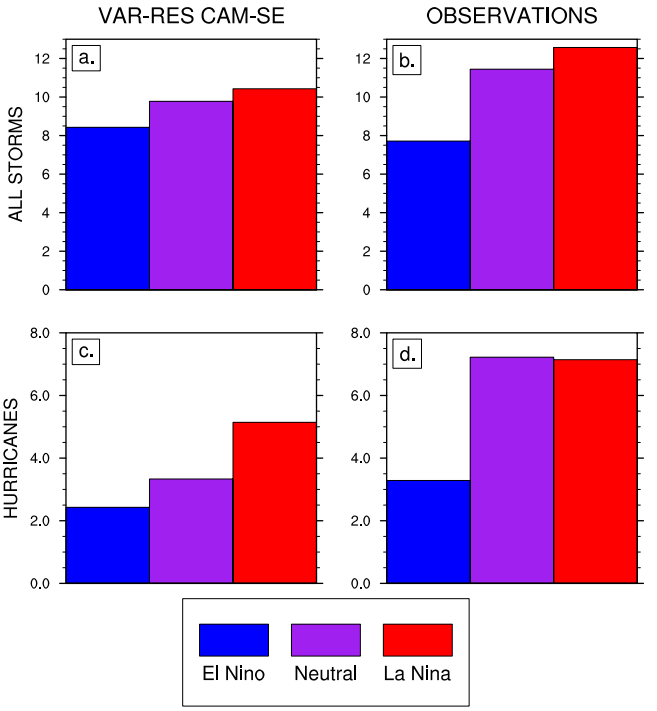

Figure 12. Bar chart showing the average number of storms (per year) that form in both El Nino and La Nina ENSO phases, as well as neutral years. Var-res CAM-SE results are (a, c) on the left with observations (b, d) on the right. All TCs are shown in top (Figures 12a and 12b) with only hurricanes on the bottom (Figures 12c and 12d).

achieve statistical significance at levels greater than 90%. Interestingly, the statistic with the highest correlation is annual major hurricane days (0.36, significant at 90%). Along with further confirmation of CAM-SE's ability to generate intense TCs at 0.25° resolution, it may also imply that intense storms have a stronger interannual signal in climate models at these grid spacings. This may be a future research question of interest as high-resolution global simulations become more prevalent in the climate community over the coming decade.

4.6.2. ENSO

It is well known that Atlantic tropical cyclone storm counts are intrinsically tied to the El Niño-Southern Oscillation (ENSO) [*Gray*, 1984]. In particular, El Niño (La Niña) events lead to stronger (weaker) westerly winds and therefore stronger (weaker) vertical wind shear over much of the Atlantic basin, leading to suppressed (enhanced) TC activity.

Figure 12 shows the average number of Atlantic TCs (top) and hurricanes (bottom) that form in the warm (El Niño), neutral, and cold (La Niña) phases of ENSO for the var-res simulation (left) and observations (right). The observed relationship between ENSO phase and TC activity (Figure 12b) is well simulated by the var-res model run (Figure 12a), with overall magnitudes as well as the bias relative to neutral years being approximately equal to those seen in observations. When TCs that do not attain hurricane strength are removed (Figures 12c and 12d), the same trends are apparent, although the model shows a larger difference between neutral and La Niña years than observed. The low bias in Atlantic hurricane activity is also evident, with the raw average totals in each ENSO phase from the model simulation being lower than the corresponding phase in the observational data set.

4.6.3. Genesis Potential Index

To assess the synoptic scale setup in the models, we utilize the Genesis Potential Index (GPI). The version of GPI used is described in *Emanuel and Nolan* [2004]. GPI has shown to be a good predictor of the seasonal cyclone of tropical cyclone activity in individual ocean basins [*Camargo et al.*, 2007]. It includes four criteria which are determined to be important to cyclogenesis and is calculated as follows:

$$\mathrm{GPI} = |10^5 \eta|^{\frac{3}{2}} \left(\frac{RH_{600}}{50}\right)^3 \left(\frac{V_{pot}}{70}\right)^3 (1+0.1|V_{shear}|)^{-2} \tag{2}$$

Here η is the 850 hPa absolute vorticity (s^{-1}), RH_{600} is the 600 hPa relative humidity (%), V_{pot} is the potential wind speed intensity (m s^{-1}), and $|V_{shear}|$ is the magnitude of the deep-layer vertical wind shear between 850 and 200 hPa (m s^{-1}). V_{pot} is defined using the formulation described in *DeMaria and Kaplan* [1994]. Note that the physical units are omitted when using equation (2) such that GPI is dimensionless.

GPI is calculated over the entirety of each individual ocean basin. *Bruyère et al.* [2012] showed that the GPI over more localized regions (such as the Atlantic MDR) is more closely correlated with TC activity, but we only seek to quantify the broad synoptic patterns over the entirety of the refined area. Table 4 shows time series correlation coefficients between the var-res simulation and NCEP Reanalysis I for both the North Atlantic and East

Table 4. Correlation Between GPI Calculated From NCEP Reanalysis and Var-res Simulation for Both the North Atlantic (NATL) and East Pacific (EPAC) Basins[a]

Basin	Monthly	Ann. Avg.	TC Season
NATL	0.85**	0.41*	0.57**
EPAC	0.82**	0.50*	0.42*

[a]Correlations statistically significant at the 99% level (**) and 95% (*) using one-sided Student's *t* test are marked.

Pacific (basins affected by refinement). Each basin has three correlation coefficients. The first is the full monthly time series (276 data points). The second and third are the annual calendar average and tropical cyclone season average, respectively (23 points). The tropical cyclone season statistic only averages over months considered to have potential tropical cyclone activity (June through December in the North Atlantic, etc.).

Both the North Atlantic (NATL) and the East Pacific (EPAC) show high correlation between the var-res simulation and observational data. These areas are climatologically active but also are likely to be more data rich, lending to a more accurate reanalysis as well as better SST fields given to CAM. Other ocean basins (not shown) showed positive but slightly weaker correlation (in some cases not significant at 95%). This may be due to these basins being more data sparse.

Table 5 shows the same analysis as Table 4 except the var-res simulation is correlated to the globally uniform 1° coarse simulation instead of reanalysis data. Note that the two AMIP simulations are forced with identical SSTs but slightly vary in atmospheric grid positions and topography roughness. The highly correlated values in Table 5 indicate that the addition of high resolution in the var-res simulation does not significantly alter the large-scale synoptic environment. Both basins are well correlated at the 99% confidence level for all three time series, showing the model produces similar atmospheric states regardless of the presence of the refined nest. In addition, all of the correlations shown in Table 5 are higher than their corresponding values in Table 4, highlighting the model is more highly correlated to an unrefined version of itself rather than reanalysis data.

4.7. Extratropical Transition and Upscale Effects

Better resolution of tropical cyclones in VRGCMs may also allow for these TCs to impact the global circulation through meridional transport of momentum, heat, and moisture. Coarse global models which do not resolve high-intensity TCs and one-way nested LAMs are unable to allow for this feedback. *Hart* [2011] found that seasons with low numbers of Atlantic TCs which recurve to the east in midlatitudes have anomalously high values of meridional heat flux in midlatitudes during the following winter, implying recurving TCs play an important role in the poleward redistribution of energy. Recent work has also shown that recurving TCs have significant downstream impacts which may span multiple ocean basins [*Harr*, 2010, and references therein].

It is clear from Figures 2a and 2b that there are essentially no recurving TCs of significant intensity in the uniform 1° simulation, whereas there are numerous intense recurvatures in the variable-resolution simulation. Additionally, the magnitudes of the meridional transient eddy transport of both zonal and meridional momentum are smallest during boreal summer due to the reduced temperature gradient between the tropics and polar region [*Holopainen*, 1967]. Therefore, it is plausible that the signature of recurving TCs may be significant enough to appear when comparing simulated northward transport between the two model simulations during the Atlantic hurricane season (August–September–October, ASO).

Table 6 summarizes the spatially averaged ASO meridional fluxes for momentum, heat, and moisture at 500 hPa due to transient eddies. Values are calculated using the method outlined in *Peixoto and Oort* [1992]. Averages are taken over the area from 40°N to 60°N and 70°W to 10°W and over the 23 year period of the simulations. The area was selected because it is at the boundary of the high-resolution nest and spans an area where extratropical transitions of TCs generally occur. Northward flux magnitudes for each quantity are greater in the variable-resolution simulation, indicating enhanced meridional transport due to transient atmospheric features (such as tropical cyclones). Cursory tests of the same analysis over the Western North Pacific (where the model is at the same resolution in both cases) show differences which are approximately an order of magnitude smaller that do not share a consistent sign (not shown), lending credence to the notion that the increased

Table 5. Same as Table 4 Except Showing Correlation Between the var-res Simulation and Global 1° Coarse Simulation

Basin	Monthly	Ann. Avg.	TC Season
NATL	0.97**	0.93**	0.93**
EPAC	0.92**	0.84**	0.72**

Table 6. Average Transient Meridional Eddy Fluxes During the ASO Period[a]

Variable	Units	Var-res	Uniform	Δ_{VR-Uni}
$\overline{V'V'}$	m2 s−2	102.5	97.2	5.3
$\overline{V'U'}$	m2 s−2	7.5	4.7	2.8
$\overline{V'T'}$	K m s−1	3.1	2.2	0.9
$\overline{V'Q'}$	kg m kg^{-1} s^{-1}	1.92×10^{-3}	1.90×10^{-3}	2.0×10^{-5}

[a]Deviations from the temporal average are denoted by a prime and the overbar represents a time average of the product. An area-weighted spatial average is then taken between 40°N to 60°N and 70°W to 10°W. Δ_{VR-Uni} is the difference between the two simulations, with positive values signaling enhanced northward transport in the variable-resolution simulation.

transport of these quantities is due to the presence of the high-resolution nest.

Figure 13 shows the spatial pattern of the difference (variable-resolution minus uniform 1°) of the ASO meridional transient eddy fluxes in Table 6. An overlay of the variable-resolution TC tracks is shown in black. Trajectories extend further northward than those in Figure 2b because vorticity maxima are now tracked beyond 45°N to better capture storms during and just after extratropical transition. Only TCs from the first half of the 23 year simulation period are plotted to decrease the density of trajectories and make the plots readable. TCs from the second half of the simulation exhibit similar trajectories.

For the northward flux of both zonal and meridional momentum (Figures 13a and 13b), the differences over the North Atlantic are positive and are centered in the area where recurving tropical cyclones are prevalent. This indicates that these storms may be playing a key role in depositing momentum and energy northward. The spatial signal is not quite as strong in either transient meridional eddy transport of temperature or moisture during ASO (Figures 13c and 13d) and negative differences appear on the western side of the basin. However, both show an area-averaged positive anomaly over the center of the basin.

The results here taken in combination with Figure 2 (which shows a high density of strong, recurving TCs into the midlatitudes and out of the high-resolution nest) imply that variable-resolution grids may help provide "upscale" effects to the global circulation. These effects are not achievable through one-way LAM nesting (which does not allow for exiting atmospheric features to influence the global circulation via boundary conditions) or coarser climate model simulations (which cannot dynamically resolve intense TCs). This is physically consistent with the idea that recurving TCs can be significant contributors to the transport of momentum, heat, and moisture from the tropics to mid and high latitudes. However, given the simplicity of this analysis, it is unclear as to the exact contribution of TCs to these budgets is. While this preliminary investigation is interesting, further work is necessary to determine if these effects and their impact on the global budget of momentum, heat, and moisture are significant.

5. Discussion and Conclusions

This paper presents a global climate simulation using the variable-resolution option of the Community Atmosphere Model's Spectral Element (CAM-SE) dynamical core. The addition of a 0.25° refined nest over the North Atlantic basin within a 1° global grid adds increased skill to simulated tropical cyclone climatology at the regional scale. Additionally, the use of variable-resolution significantly decreases the computational cost required to complete a simulation. In the high-resolution nest, the average storm climatology is dramatically improved when compared to the use of a global coarse grid. The average TC count closely matches observations while the high-resolution nest allows for the direct simulation of intense cyclones with maximum wind speeds up to approximately 80 m s^{-1}.

While this study was not directly compared to a globally uniform high-resolution run due to the large computational expense that would be required for such a simulation, *Zarzycki et al.* [2014b] showed that localized refinement patches in CAM-SE closely matched the climatology from those regions within a globally uniform high-resolution run in aquaplanet simulations. *Wehner et al.* (submitted manuscript, 2014) and *Bacmeister et al.* [2014] also show similar TC statistics in globally uniform 0.25° CAM Finite Volume (FV) simulations. These results in aggregate indicate that the high-resolution patch within our variable-resolution framework does a sufficient job reproducing the climatology of a 0.25° globally uniform grid over the Atlantic basin.

These results also underscore the critical necessity for high resolution (less than 50 km horizontal grid spacing) to properly resolve the dynamical structure of TCs. However, it is interesting that CAM simulates a very realistic distribution of TC intensities at 0.25° grid spacing. While this resolution is considered very high for climate simulations, it remains well coarser than resolutions required for studying more fine-scale aspects of

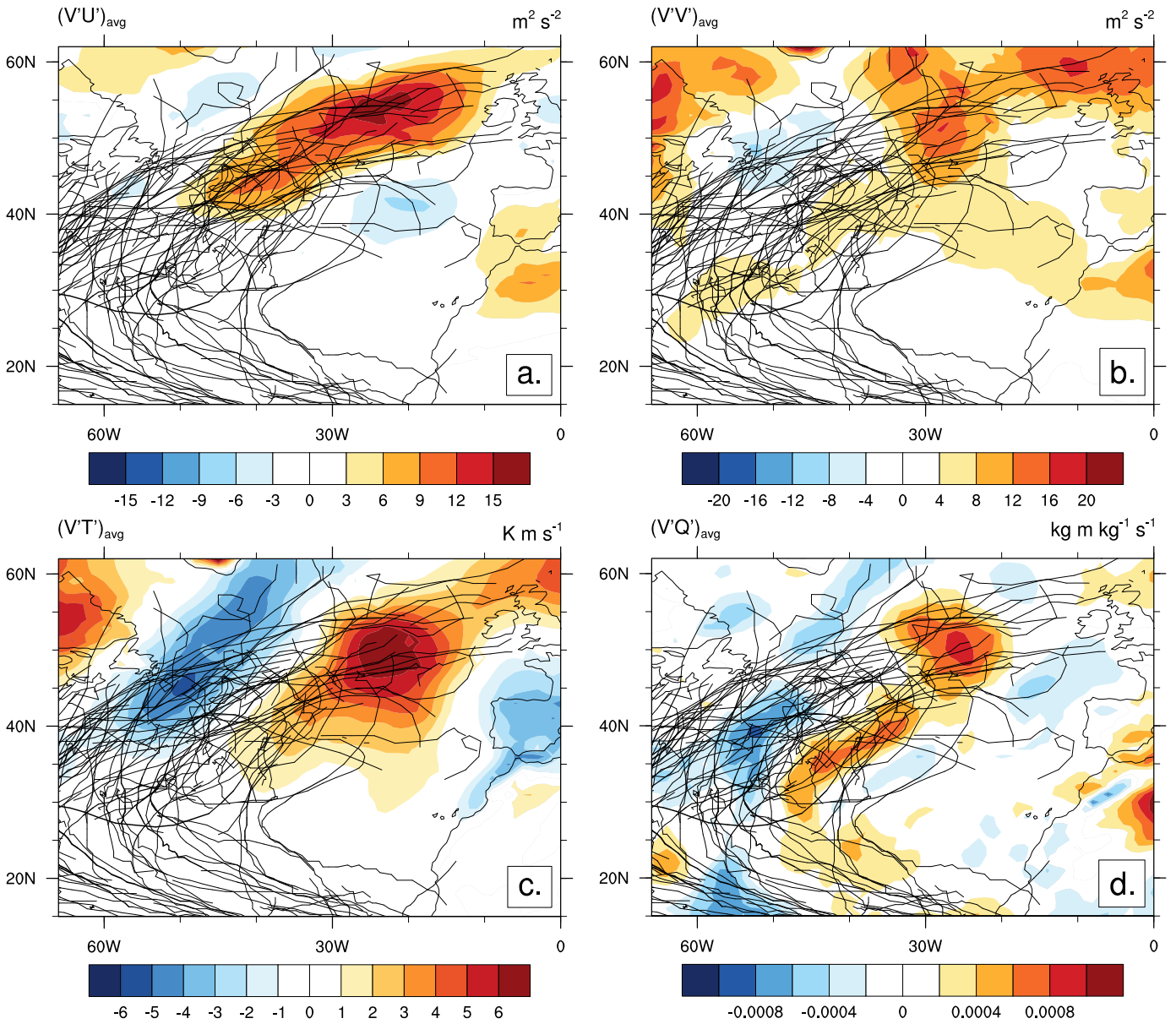

Figure 13. Differences in ASO transient meridional (northward) eddy fluxes of (a) zonal momentum, (b) meridional momentum, (c) temperature, and (d) moisture between the variable-resolution and uniform 1° solutions. Difference is calculated as variable-resolution minus uniform 1°. Extended TC tracks from the variable-resolution simulation are marked in black to demonstrate recurvature region.

tropical cyclone dynamics such as eyewall asymmetries [*Persing et al.*, 2013] and vortical hot towers [*Hendricks et al.*, 2004]. Cursory simulations using a similar variable-resolution CAM setup with 0.125° grid spacing show that some TCs in the Atlantic reach minimum surface pressures below 890 hPa which are unrealistically low. *Reed et al.* [2012] also found that at higher resolutions, CAM-SE with CAM5 physics produced tropical cyclones which exceeded their maximum potential intensity. This result may mean further tuning or modification of physical parameterizations is necessary for long-term, high-resolution simulations within CAM. It also emphasizes that TC development critically depends on the nonlinear interactions between the dynamical core and subgrid parameterizations such as convection and surface fluxes. Future work will continue to investigate the performance of these parameterizations at high resolutions and suggest potential modifications required for further improvement in TC representation as model resolutions push finer.

These strong intensities may also result from the specification of fixed SSTs. In nature, tropical storms remove heat from the ocean surface through flux extraction and turbulent mixing of the upper ocean which draws cooler water upward [*Price*, 1981; *Emanuel*, 2001]. This cooling reduces sensible and latent heat available to the TC and thereby provides a negative feedback on its intensity. As this cooling increases with increased surface stress (faster wind speed), this governing mechanism is stronger for higher intensity storms. With climate models now able to produce category 4 and higher intensities [e.g., this study, *Manganello et al*., 2012; *Satoh et al*., 2012; Wehner et al. (submitted manuscript, 2014)], the practice of using fixed, prescribed SSTs likely needs to be re-evaluated for high-resolution climate simulations.

As shown in section 4.6, while the variable-resolution simulation does an adequate job simulating average TC statistics, it struggles to produce high correlation statistics when individual model years are compared to observations. These difficulties are interesting given the fact that past work with ensembles of global models at lower resolutions (50–100 km) found very high correlations (>0.7) between modeled TCs and observations in the Atlantic basin without internally nudging synoptic scales [e.g., *LaRow et al*., 2008; *Zhao et al*., 2009]. This result is unlikely to indicate a deficiency in the variable-resolution setup. For example, Wehner et al. (submitted manuscript, 2014) and *Bacmeister et al*. [2014] also found similar correlations between modeled cyclone count and observations when using AMIP protocols and CAM-FV with CAM5 physics. The model is able to reproduce the Atlantic cyclone teleconnection to ENSO events, implying that some component of the prescribed SST signal affects Atlantic TC formation. Therefore, it is unknown whether there exists an inherent issue with the flow of information from the ocean surface to the atmosphere which is specific to CAM or whether this lower correlation is the result of using a single simulation as compared to an ensemble. One advantage to developing a variable-resolution global model is the decrease in computational assets required for a single simulation that focuses on a regional phenomenon. As shown in *Zarzycki et al*. [2014a, 2014b], the runtime of CAM-SE essentially scales linearly with the number of grid elements. This provides obvious potential for VRGCMs to be used for multimember ensemble studies instead of single, globally uniform, high-resolution model runs for the same computational cost. Therefore, future work will include developing an ensemble of AMIP simulations with variable-resolution meshes to evaluate if skill in reproducing interannual variation in cyclone counts and intensity over the historical time period is improved.

Also, while this paper focuses on tropical cyclones, a companion paper analyzes the large-scale climatological statistics within the variable-resolution model. Similar to the GPI results here, analysis shows that certain resolution-specific effects such as topographical features and high-intensity precipitation events are improved in the high-resolution nest while the global statistics remain unaffected by the addition of resolution. These conclusions provide evidence that VRGCMs may be useful multiscale tools to improve regional climate assessments, even without significant development of novel parameterizations, in the near future. In the long run, however, special attention needs to be paid to the performance of physical parameterizations across scales.

Acknowledgments

This research was supported by the Office of Science, U.S. Department of Energy (DoE), Award Nos. DE-SC0003990 and DE-SC0006684. The authors thank Mark A. Taylor for his assistance with running CAM-SE, Peter H. Lauritzen for his help with generating variable-resolution topography data sets, and Michael F. Wehner for providing code which became the base for the cyclone tracking algorithm as well as fruitful discussions regarding high-resolution CAM simulations. They would also like to thank an anonymous reviewer for helpful comments regarding this manuscript. Some of this work was completed while C.M.Z. was an invited attendee of the "Multiscale Numerics for the Atmosphere and Ocean" programme at the Isaac Newton Institute for Mathematical Sciences in Cambridge, United Kingdom. The majority of the high performance computing support for this project was provided by NCAR's Computational and Information Systems Laboratory which is sponsored by the National Science Foundation. The authors thank Paul A. Ullrich for providing access to computing resources at the University of California, Davis to complete supporting portions of this work. Model data used in this study are currently stored using resources from NCAR's Computational and Information Systems Laboratory and can be obtained by contacting the corresponding author.

References

Abiodun, B. J., J. M. Prusa, and W. J. Gutowski (2008), Implementation of a non-hydrostatic, adaptive-grid dynamics core in CAM3. Part I: Comparison of dynamics cores in aqua-planet simulations, *Clim. Dyn.*, *31*(7–8), 795–810.

Anderson, B. D., S. E. Benzley, and S. J. Owen (2009), Automatic all quadrilateral mesh adaption through refinement and coarsening, in *Proceedings of the 18th International Meshing Roundtable*, edited by B. W. Clark, pp. 557–574, Springer, Berlin.

Atkinson, G. D., and C. R. Holliday (1977), Tropical cyclone minimum sea level pressure/maximum sustained wind relationship for the western North Pacific, *Mon. Weather Rev.*, *105*(4), 421–427.

Bacmeister, J. T., M. F. Wehner, R. B. Neale, A. Gettelman, C. Hannay, P. H. Lauritzen, J. M. Caron, and J. E. Truesdale (2014), Exploratory high-resolution climate simulations using the Community Atmosphere Model (CAM), *J. Clim.*, *27*(9), 3073–3099, doi:10.1175/JCLI-D-13-00387.1.

Bell, G. D., et al. (2000), Climate assessment for 1999, *Bull. Am. Meteorol. Soc.*, *81*, 1328–1328, doi:10.1175/1520-0477(2000)081<1328:CAF>2.3.CO;2.

Bengtsson, L., K. I. Hodges, and M. Esch (2007), Tropical cyclones in a T159 resolution global climate model: Comparison with observations and re-analyses, *Tellus, Ser. A*, *59*(4), 396–416, doi:10.1111/j.1600-0870.2007.00236.x.

Bruyère, C. L., G. J. Holland, and E. Towler (2012), Investigating the use of a genesis potential index for tropical cyclones in the north Atlantic basin, *J. Clim.*, *25*(24), 8611–8626, doi:10.1175/JCLI-D-11-00619.1.

Camargo, S., A. Sobel, A. Barnston, and K. Emanuel (2007), Tropical cyclone genesis potential index in climate models, *Tellus, Ser. A*, *59*(4), 428–443.

Camargo, S. J., and S. E. Zebiak (2002), Improving the detection and tracking of tropical cyclones in atmospheric general circulation models, *Weather Forecasting*, *17*(6), 1152–1162.

Caron, L.-P., C. G. Jones, and K. Winger (2011), Impact of resolution and downscaling technique in simulating recent Atlantic tropical cyclone activity, *Clim. Dyn.*, *37*(5–6), 869–892, doi:10.1007/s00382-010-0846-7.

Chauvin, F., J.-F. Royer, and M. Déqué (2006), Response of hurricane-type vortices to global warming as simulated by ARPEGE-Climat at high resolution, *Clim. Dyn.*, *27*(4), 377–399, doi:10.1007/s00382-006-0135-7.

Côté, J., M. Roch, A. Staniforth, and L. Fillion (1993), A variable-resolution semi-Lagrangian finite-element global-model of the shallow-water equations, *Mon. Weather Rev.*, *121*(1), 231–243.
Craig, A. P., M. Vertenstein, and R. Jacob (2012), A new flexible coupler for earth system modeling developed for CCSM4 and CESM1, *Int. J. High Performance Comput. Appl.*, *26*(1), 31–42, doi:10.1177/1094342011428141.
DeMaria, M., and J. Kaplan (1994), Sea surface temperature and the maximum intensity of Atlantic tropical cyclones, *J. Clim.*, *7*(9), 1324–1334, doi:10.1175/1520-0442(1994)007<1324:SSTATM>2.0.CO;2.
Dennis, J. M., J. Edwards, K. J. Evans, O. Guba, P. H. Lauritzen, A. A. Mirin, A. St-Cyr, M. A. Taylor, and P. H. Worley (2012), CAM-SE: A scalable spectral element dynamical core for the Community Atmosphere Model, *Int. J. High Performance Comput. Appl.*, *26*(1), 74–89, doi:10.1177/1094342011428142.
Emanuel, K. (2001), Contribution of tropical cyclones to meridional heat transport by the oceans, *J. Geophys. Res.*, *106*(D14), 14,771–14,781.
Emanuel, K. A., and D. Nolan (2004), Tropical cyclone activity and the global climate system, *Preprints, 26th Conf. on Hurricanes and Tropical Meteorology*, Miami, FL, Amer. Meteor. Soc., 10A.2. [Available online at https://ams.confex.com/ams/26HURR/techprogram/paper_75463.htm].
Evans, K. J., P. H. Lauritzen, S. K. Mishra, R. B. Neale, M. A. Taylor, and J. J. Tribbia (2013), AMIP simulation with the CAM4 spectral element dynamical core, *J. Clim.*, *26*(3), 689–709, doi:10.1175/JCLI-D-11-00448.1.
Flato, G., et al. (2013), Evaluation of climate models, in *Climate Change 2013: The Physical Science Basis. Contribution of Working Group I to the Fifth Assessment Report of the Intergovernmental Panel on Climate Change*, edited by T. Stocker et al., pp. 741–866, Cambridge Univ. Press, Cambridge, U. K.
Frank, W. M. (1977), The structure and energetics of the tropical cyclone I. Storm structure, *Mon. Weather Rev.*, *105*(9), 1119–1135.
Garratt, J. R. (1992), *The Atmospheric Boundary Layer*, 316 pp., Cambridge Univ. Press, Cambridge, U. K.
Gates, W. L. (1992), AMIP: The Atmospheric Model Intercomparison Project, *Bull. Am. Meteorol. Soc.*, *73*, 1962–1970.
Giammanco, I. M., J. L. Schroeder, and M. D. Powell (2012), Observed characteristics of tropical cyclone vertical wind profiles, *J. Wind Struct.*, *15*, 1–22.
Gray, W. M. (1984), Atlantic seasonal hurricane frequency. Part I: El Niño and 30 mb Quasi-Biennial Oscillation influences, *Mon. Weather Rev.*, *112*(9), 1649–1668, doi:10.1175/1520-0493(1984)112<1649:ASHFPI>2.0.CO;2.
Guishard, M. P., J. L. Evans, and R. E. Hart (2009), Atlantic subtropical storms. Part II: Climatology, *J. Clim.*, *22*(13), 3574–3594.
Hamilton, K. (2008), Numerical resolution and modeling of the global atmospheric circulation: A review of our current understanding and outstanding issues, in *High Resolution Numerical Modelling of the Atmosphere and Ocean*, edited by K. Hamilton and W. Ohfuchi, pp. 7–27, Springer, New York, doi:10.1007/978-0-387-49791-4_1.
Harper, B. A., J. D. Kepert, and J. D. Ginger (2010), Guidelines for converting between various wind averaging periods in tropical cyclone conditions, Tech. Rep. WMO/TD-1555, World Meteorol. Organ.
Harr, P. A. (2010), The extratropical transition of tropical cyclones: Structural characteristics, downstream impacts, and forecast challenges, in *Global Perspectives on Tropical Cyclones: From Science to Mitigation, vol. 4*, edited by J. C. L. Chan and J. D. Kepert, p. 436, World Sci, Singapore.
Harris, L. M., and S.-J. Lin (2013), A two-way nested global-regional dynamical core on the cubed-sphere grid, *Mon. Weather Rev.*, *141*(1), 283–306.
Hart, R. E. (2011), An inverse relationship between aggregate northern hemisphere tropical cyclone activity and subsequent winter climate, *Geophys. Res. Lett.*, *38*, L01705, doi:10.1029/2010GL045612.
Hazelton, A. T., and R. E. Hart (2012), Hurricane eyewall slope as determined from airborne radar reflectivity data: Composites and case studies, *Weather Forecasting*, *28*(2), 368–386, doi:10.1175/WAF-D-12–00037.1.
Hendricks, E. A., M. T. Montgomery, and C. A. Davis (2004), The role of "vortical" hot towers in the formation of tropical cyclone Diana (1984), *J. Atmos. Sci.*, *61*(11), 1209–1232, doi:10.1175/1520-0469(2004)061<1209:TROVHT>2.0.CO;2.
Holopainen, E. O. (1967), On the mean meridional circulation and the flux of angular momentum over the northern hemisphere, *Tellus*, *19*(1), 1–13, doi:10.1111/j.2153-3490.1967.tb01453.x.
Hurrell, J. W., J. J. Hack, D. Shea, J. M. Caron, and J. Rosinski (2008), A new sea surface temperature and sea ice boundary dataset for the Community Atmosphere Model, *J. Clim.*, *21*(19), 5145–5153, doi:10.1175/2008JCLI2292.1.
Kalnay, E., et al. (1996), The NCEP/NCAR 40-year reanalysis project, *Bull. Am. Meteorol. Soc.*, *77*(3), 437–471, doi:10.1175/1520-0477(1996)077<0437:TNYRP>2.0.CO;2.
Knaff, J. A., and R. M. Zehr (2007), Reexamination of tropical cyclone wind-pressure relationships, *Weather Forecasting*, *22*(1), 71–88, doi:10.1175/WAF965.1.
Knapp, K. R., M. C. Kruk, D. H. Levinson, H. J. Diamond, and C. J. Neumann (2010), The international best track archive for climate stewardship (IBTrACS), *Bull. Am. Meteorol. Soc.*, *91*(3), 363–376, doi:10.1175/2009BAMS2755.1.
Knutson, T. R., J. J. Sirutis, S. T. Garner, I. M. Held, and R. E. Tuleya (2007), Simulation of the recent multidecadal increase of Atlantic hurricane activity using an 18-km-grid regional model, *Bull. Am. Meteorol. Soc.*, *88*, 1549, doi:10.1175/BAMS-88-10-1549.
Landsea, C. W., G. A. Vecchi, L. Bengtsson, and T. R. Knutson (2009), Impact of duration thresholds on Atlantic tropical cyclone counts, *J. Clim.*, *23*(10), 2508–2519, doi:10.1175/2009JCLI3034.1.
LaRow, T. E., Y.-K. Lim, D. W. Shin, E. P. Chassignet, and S. Cocke (2008), Atlantic basin seasonal hurricane simulations, *J. Clim.*, *21*(13), 3191–3206, doi:10.1175/2007JCLI2036.1.
Lauritzen, P. H., J. Bacmeister, M. A. Taylor, and R. B. Neale (2012), *New CAM (NSF-DOE Community Atmosphere Model) topography generation software: CAM5.2, Abstract A53C-0157 presented at 2012 Fall Meeting*, AGU, San Francisco, Calif., 3–7 Dec.
Lauritzen, P. H., J. T. Bacmeister, T. Dubos, S. Lebonnois, and M. A. Taylor (2014), Held-Suarez simulations with the Community Atmosphere Model Spectral Element (CAM-SE) dynamical core: A global axial angular momentum analysis using Eulerian and floating Lagrangian vertical coordinates, *J. Adv. Model. Earth Syst.*, *6*, 129–140, doi:10.1002/2013MS000268.
Manganello, J. V., et al. (2012), Tropical cyclone climatology in a 10-km global atmospheric GCM: Toward weather-resolving climate modeling, *J. Clim.*, *25*(11), 3867–3893, doi:10.1175/JCLI-D-11-00346.1.
Mendelsohn, R., K. Emanuel, S. Chonabayashi, and L. Bakkensen (2012), The impact of climate change on global tropical cyclone damage, *Nat. Clim. Change*, *2*(3), 205–209.
Mesinger, F., and K. Veljovic (2013), Limited area NWP and regional climate modeling: A test of the relaxation vs Eta lateral boundary conditions, *Meteorol. Atmos. Phys.*, *119*(1–2), 1–16, doi:10.1007/s00703-012-0217-5.
Murakami, H., et al. (2012), Future changes in tropical cyclone activity projected by the new high-resolution MRI-AGCM, *J. Clim.*, *25*(9), 3237–3260, doi:10.1175/JCLI-D-11-00415.1.
Neale, R. B., et al. (2010), Description of the NCAR Community Atmosphere Model (CAM 5.0), NCAR Technical Note NCAR/TN-486+STR, Natl. Cent. for Atmos. Res., Boulder, Colo.

Oouchi, K., J. Yoshimura, H. Yoshimura, R. Mizuta, S. Kusunoki, and A. Noda (2006), Tropical cyclone climatology in a global-warming climate as simulated in a 20 km-mesh global atmospheric model: Frequency and wind intensity analyses, *J. Meteorol. Soc. Jpn.*, *84*(2), 259–276.

Peixoto, J. P., and A. H. Oort (1992), *Physics of Climate*, 520 pp., Am. Inst. of Phys., New York.

Persing, J., M. T. Montgomery, J. C. McWilliams, and R. K. Smith (2013), Asymmetric and axisymmetric dynamics of tropical cyclones, *Atmos. Chem. Phys. Discuss.*, *13*(5), 13,323–13,438, doi:10.5194/acpd-13-13323-2013.

Price, J. F. (1981), Upper ocean response to a hurricane, *J. Phys. Oceanogr.*, *11*(2), 153–175.

Reed, K. A., C. Jablonowski, and M. A. Taylor (2012), Tropical cyclones in the spectral element configuration of the Community Atmosphere Model, *Atmos. Sci. Lett.*, *13*(4), 303–310.

Ringler, T., L. Ju, and M. Gunzburger (2008), A multiresolution method for climate system modeling: Application of spherical centroidal Voronoi tessellations, *Ocean Dyn.*, *58*, 475–498.

Satoh, M., et al. (2012), The intra-seasonal oscillation and its control of tropical cyclones simulated by high-resolution global atmospheric models, *Clim. Dyn.*, *39*(9–10), 2185–2206, doi:10.1007/s00382-011-1235-6.

Simpson, R. H. (1974), The hurricane disaster—Potential scale, *Weatherwise*, *27*(4), 169–186, doi:10.1080/00431672.1974.9931702.

Skamarock, W. C., J. B. Klemp, M. G. Duda, L. D. Fowler, S.-H. Park, and T. D. Ringler (2012), A multiscale nonhydrostatic atmospheric model using centroidal Voronoi tesselations and C-grid staggering, *Mon. Weather Rev.*, *140*(9), 3090–3105, doi:10.1175/MWR-D-11-00215.1.

Strachan, J., P. L. Vidale, K. Hodges, M. Roberts, and M.-E. Demory (2013), Investigating global tropical cyclone activity with a hierarchy of AGCMs: The role of model resolution, *J. Clim.*, *26*(1), 133–152, doi:10.1175/JCLI-D-12-00012.1.

Strazzo, S., J. B. Elsner, T. LaRow, D. J. Halperin, and M. Zhao (2013), Observed versus GCM-generated local tropical cyclone frequency: Comparisons using a spatial lattice, *J. Clim.*, *26*(21), 8257–8268, doi:10.1175/JCLI-D-12–00808.1.

Taylor, M., J. Tribbia, and M. Iskandarani (1997), The spectral element method for the shallow water equations on the sphere, *J. Comput. Phys.*, *130*, 92–108.

Taylor, M. A. (2011), Conservation of mass and energy for the moist atmospheric primitive equations on unstructured grids, in Numerical Techniques for Global Atmospheric Models, Lecture Notes in Computational Science and Engineering, *vol. 80*, edited by P. H. Lauritzen et al., pp. 357–380, Springer, Berlin, Germany.

Taylor, M. A., and A. Fournier (2010), A compatible and conservative spectral element method on unstructured grids, *J. Comput. Phys.*, *229*(17), 5879–5895.

Tomita, H. (2008), A stretched icosahedral grid by a new grid transformation, *J. Meteorol. Soc. Jpn.*, *86*(0), 107–119.

Vitart, F., J. L. Anderson, and W. F. Stern (1997), Simulation of interannual variability of tropical storm frequency in an ensemble of GCM integrations, *J. Clim.*, *10*(4), 745–760.

Walko, R. L., and R. Avissar (2011), A direct method for constructing refined regions in unstructured conforming triangular–hexagonal computational grids: Application to OLAM, *Mon. Weather Rev.*, *139*(12), 3923–3937, doi:10.1175/MWR-D-11-00021.1.

Walsh, K., S. Lavender, E. Scoccimarro, and H. Murakami (2013), Resolution dependence of tropical cyclone formation in CMIP3 and finer resolution models, *Clim. Dyn.*, *40*(3–4), 585–599, doi:10.1007/s00382-012-1298-z.

Warner, T. T., R. A. Peterson, and R. E. Treadon (1997), A tutorial on lateral boundary conditions as a basic and potentially serious limitation to regional numerical weather prediction, *Bull. Am. Meteorol. Soc.*, *78*(11), 2599–2617.

Wieringa, J. (1992), Updating the Davenport roughness classification, *J. Wind Eng. Ind. Aerodyn.*, *41*(1–3), 357–368, doi:10.1016/0167-6105(92)90434-C.

Williamson, D. L. (2013), The effect of time steps and time-scales on parametrization suites, *Q. J. R. Meteorol. Soc.*, *139*(671), 548–560, doi:10.1002/qj.1992.

Zarzycki, C. M., C. Jablonowski, and M. A. Taylor (2014a), Using variable resolution meshes to model tropical cyclones in the Community Atmosphere Model, *Mon. Weather Rev.*, *142*(3), 1221–1239, doi:10.1175/MWR-D-13-00179.1.

Zarzycki, C. M., M. N. Levy, C. Jablonowski, J. R. Overfelt, M. A. Taylor, and P. A. Ullrich (2014b), Aquaplanet experiments using CAM's variable-resolution dynamical core, *J. Clim.*, *27*(14), 5481–5503, doi:10.1175/JCLI-D-14-00004.1.

Zhao, M., I. M. Held, S. J. Lin, and G. A. Vecchi (2009), Simulations of global hurricane climatology, interannual variability, and response to global warming using a 50-km resolution GCM, *J. Clim.*, *22*(24), 6653–6678.

Zhao, M., I. M. Held, and S.-J. Lin (2012), Some counterintuitive dependencies of tropical cyclone frequency on parameters in a GCM, *J. Atmos. Sci.*, *69*(7), 2272–2283, doi:10.1175/JAS-D-11-0238.1.